PNAS

Supplementary Materials for

Deficiency of orexin signaling during sleep is involved in abnormal REM sleep architecture in narcolepsy

Hiroto Ito[1, 2, 3], Noriaki Fukatsu[1, 2], Sheikh Mizanur Rahaman[1, 2], Yasutaka Mukai[1, 2], Shuntaro Izawa[1, 2], Daisuke Ono[1, 2], Thomas S. Kilduff[4], *Akihiro Yamanaka[1,2,5,6,7]

Akihiro Yamanaka
Email: yamank@cibr.ac.cn

This PDF file includes:

Supplementary Materials and Methods
Supplementary Figures 1 to 15
Captions for Movies S1 to S4
Supplementary Tables 1 to 3

Other Supplementary Materials for this manuscript include the following:

Movies S1 to S4
Dataset S1

Supplementary Materials and Methods

Animals

All experimental protocols involving the use of mice were approved by the Institutional Animal Care and Use Committees, Research Institute of Environmental Medicine, Nagoya University, Japan (#19232 and #19268) and SRI International (#01026). All efforts were made to reduce the number of mice used and to minimize the pain and suffering of mice. *Orexin-tTA* (1), *orexin-Flp* (2), and *TetO-ChR2* (3) mice were used in this study. These mice were maintained on a C57BL/6J genetic background. C57BL/6J mice were used as wild-type mice. Adult mice (2 to 5 months at the time of surgery) of both sexes were studied, except for the optogenetic experiments in which only male mice were used. Animals were maintained in home cages on a 12-hour light-dark cycle (8:00-20:00). The environmental temperature was 23 ± 2°C with food and water provided *ad libitum*.

AAV production and injection

Using the AAV Helper-Free System (Agilent Technologies, Inc., Santa Clara, CA, USA), adeno-associated viral (AAV) vectors were produced and purified based on a previously published protocol (4, 5). Briefly, HEK293 cells were transfected with pAAV vector plasmid that included a gene of interest, pHelper (Agilent Technologies) and pAAV-RC (serotype 9: provided by Univ. Penn. Vector Core; DJ: Cosmo Bio Co., Ltd, Tokyo, Japan) using a standard calcium phosphate method. After 3 days, the transfected HEK293 cells were collected and suspended in Hank's balanced salt solution (H8264, Sigma-Aldrich, Tokyo, Japan). Following multiple freeze-thaw cycles, the cell lysate was treated with benzonase nuclease (Merck, Darmstadt, Germany) at 37°C for 30 min and centrifuged 2 times at 16,000 g for 10 min. The supernatant was used as the AAV-containing solution. Quantitative PCR was performed to measure the titer of the purified virus; virus aliquots were stored at -80℃ until use.

For AAV injection, mice were anesthetized with isoflurane (Wako Pure Chemical Industries) anesthesia (< 2%) and fixed in a stereotaxic frame (David Kopf Instruments). Using injectors (BJ-110; BEX CO, Ltd., Itabashi, Tokyo, Japan or Nanoject III; Drummond Scientific Company, Broomall, PA, USA), AAV was injected into the LHA at the following volumes and titers: AAV9-TetO-GCaMP6s (400-600 nl/injection, 2.1×10^{13} copies/ml), AAV9-CMV-dFRT-GCaMP6s (600 nl/injection, 7.7×10^{12} or 1.6×10^{13} copies/ml), AAV9-TetO-ArchT-EGFP (600

nl/injection, 2.2×10^{12} or 7.4×10^{12} copies/ml), AAV9-CMV-dFRT-ArchT-EGFP (600 nl/injection, 1.7×10^{12} copies/ml), AAV9-TetO-EGFP (600 nl/injection, 3.2×10^{12} copies/ml), and AAV(DJ)-CMV-dFRT-hrGFP (600 nl/injection, 3.9×10^{13} copies/ml) with a glass micropipette (tip diameter: about 60 μm [BJ-110] or about 45 μm [Nanoject III]). For optogenetic manipulation of neural activity, AAV was injected using the BJ-110 into four different sites in the hypothalamus (two injections into each hemisphere) to cover the distribution area of orexin neurons. Injection coordinates were as follows: AP=-1.4 to -1.3 mm; ML=±0.5 mm; DV=-5.4 to -5.2 mm and AP=-1.4 to -1.3 mm; ML=±0.9 mm; DV=-5.4 to -5.2 mm. For fiber photometry or nVista imaging, AAV was injected with a Nanoject III into two sites as follows: AP=-1.4 to 1.3 mm; ML=+0.9 mm; DV-5.4 to -5.2 mm and AP=-1.9 to -1.6 mm; ML=+0.9 mm; DV=-5.4 to -5.2 mm. To ensure adequate gene expression, the injected mice were not used for experiments or surgeries for at least 3 weeks after injection.

EEG/EMG Surgery and description of the sleep recording system

Procedures for implanting EEG and EMG electrodes for polysomnographic recording experiments were adapted and modified from our previously published protocol (4). Briefly, two screws (U-1430-01, Wilco, Yokohama, Japan) were implanted on the skull (AP=+0.5 to 1.0 mm; ML=-0.5 to -1.0 mm and AP=-2.5 to 3.0 mm; ML=-2.5 to -3.0 mm) to record EEG, and two stainless steel wires (209-4811, RS PRO, Yokohama, Japan) were inserted on either side of the nuchal muscle to record EMG. All screws and wires were secured to the connector pins using Super-Bond (Super-Bond C&B, Sun Medical, Moriyama, Japan) and dental cement (REPAIRSIN, GC). After at least 3 days of recovery, mice were connected to a cable through a slip ring designed such that the movement of the mouse was unrestricted, and the mice were habituated for at least another 7 days. Then, EEG and EMG recordings were conducted along with optogenetic or Ca^{2+} imaging. EEG and EMG signals were amplified (AB-610J, Nihon Kohden), filtered (EEG, 1.5-30 Hz; EMG, 15-300 Hz), digitized at a sampling rate of 128 Hz, and recorded using VitalRecorder (Kissei Comtec, Nagano, Japan). Using the SleepSign video option system (Kissei Comtec), the animal's behavior (monitored through a CCD video camera) was recorded on a computer synchronized with the EEG/EMG recordings. An infrared activity monitor sensor (Biotex, Kyoto, Japan) was set on top of the cage to detect locomotor activity. The sensor’s

signals (representing the animal's movement) were digitized and transferred to a computer.

Offline vigilance states definition using EEG and EMG recordings

EEG/EMG recordings were automatically scored in 4-sec epochs and classified as wakefulness (wake), NREM sleep, or REM sleep by SleepSign3 software (Kissei Comtec) according to standard criteria (1, 6). Three vigilance states—(1) waking (high EMG and low EEG amplitude and high theta activity concomitant with the highest EMG values), (2) NREM sleep (low EMG and high EEG amplitude, high delta activity), and (3) REM sleep (low EMG and low EEG amplitude, high theta activity)—were determined for 4-sec epochs and the scores were entered into a PC. In epochs during which the transition from NREM to REM sleep was problematic to score (an intermediate state), the epochs were classified as NREM sleep, unless they met the criteria of REM sleep. The tNR was defined as the last 30 sec during the transition from NREM to REM sleep. All vigilance state classifications assigned by SleepSign3 were examined visually and corrected if necessary. The same individual scored all EEG/EMG recordings. Epochs including visually detectable EEG artifacts were classified as the same stage as a previous epoch. In fast Fourier transform (FFT) analysis, epochs including visually detectable EEG artifacts were excluded. The vigilance state was considered to have changed when three successive epochs showed features of a different vigilance state. Cataplexy was identified using a combination of multiple criteria: muscle atonia lasting 10 sec, a predominance of theta activity with relatively low EEG amplitudes, and more than 40 sec of preceding wakefulness. We included HSPT and theta activity followed by the first short delta activity (~10 sec) as "predominance of theta activity with relatively low EEG amplitudes". The transition ratio was calculated by simply dividing the number of REM bouts by NREM bouts, i.e., the percentage of NREM sleep followed by REM sleep. Cumulative probability was calculated by summing the probabilities of the occurrence of transition (REM sleep or Wake) sequentially, based on the duration of all NREM sleep episodes in all mice. To evaluate NREM sleep without microarousal in the fiber photometry experiments, we classified brief episodes of wakefulness (~4 sec) flanked by NREM sleep as wakefulness with epochs located on both sides. Micro-arousal was defined as wakefulness within 12 sec. Spectral analysis of the EEG was performed at 128 Hz, which yielded power spectra profiles over a 0-20 Hz window with a 1 Hz resolution for

the δ (1-5 Hz), θ (6-10 Hz), and α (11-14 Hz) bandwidths. An average EEG spectral profile was calculated from the EEG power densities in each frequency bin and normalized to the maximum value of EEG spectral power during NREM sleep when orexin neuron activity is low, i.e., a low Z-score (NR; shown in Supplementary Figures 1 and 5), and to baseline recordings (Supplementary Figure 9). EEG spectrograms were analyzed using the Signal Processing Toolbox of Matlab (MathWorks, Natick, MA, USA). In the EMG in Supplementary Figure 6A, for noise removal, frequencies that were clearly outliers in the FFT analysis were removed.

HSPT detection

The definition of HSPT was adapted and modified from a previously published protocol (7). Briefly, HSPT was defined as a conspicuous, stereotypical, high-amplitude theta EEG burst, with a relatively 'pure' frequency of 6-7 Hz and a duration of 1-4 sec. Spectral analysis showed a theta power surge at 6-7 Hz. We defined these EEG events as HSPT. Any 4-sec epoch showing one or more HSPT event(s) lasting > 1 sec was scored as an HSPT bout.

Fiber photometry recordings

The fiber photometry setup (COME2-FTR/OPT, Lucir, Tsukuba, Japan) has previously been described in detail (4, 5). Briefly, we used a LED (PlexBright OPT/LED Blue_TT_FC, Plexon, Dallas, TX) for the light source. The intensity of blue (465 nm) light at the tip of the fiber was 0.07 mW (when the N.A. of the fiber was 0.39 in 3 *orexin-tTA* mice) or 0.04 mW (when the N.A. of the fiber was 0.5 in the other 8 mice). The LED-emitted excitation light was reflected by a dichroic mirror and coupled to the fiber optics (N.A. 0.5 or 0.39, 400 μm diameter) through a GFP excitation bandpass filter (path 472 ± 35 nm). GCaMP6s fluorescence was collected by the same optic fiber passed through a bandpass emission filter (path 525 ± 25 nm) and guided to a photomultiplier tube (1P28, Hamamatsu Photonics K.K., Hamamatsu, Japan). GCaMP6s signal was A/D converted and stored in a PC using Vital Recorder (Kissei Comtec Co., Ltd, Japan) together with the EEG/EMG signals at a sampling frequency of 128 Hz. At least three weeks after AAV injection, the guide cannula was stereotaxically implanted with a dummy fiber above the LHA and fixed to the skull with dental cement (REPAIRSIN, GC) and Super-bond (Super-bond C&B, Sun Medical, Moriyama, Japan) during the EEG/EMG surgery. No sooner than three days after the surgery, optic fibers were

implanted (AP=-1.4 mm; ML=+0.9 mm; DV=-4.8 to 5.0 mm). Fiber photometry recordings for 24 hours (from ZT12) were conducted no sooner than one week after the fiber implantation and habituation. After the experiment, the recorded GCaMP6s signal was smoothed by a 64-point moving average and converted to DF/F (%) as follows: $DF/F=100*(F(t)-F_{min})/F_{min}$, where F(t) is the GCaMP6s signal and F_{min} is the minimum value of the signal. To quantify the GCaMP6s signal across different animals, the ΔF/F was normalized to the Z-score using the standard deviation of the ΔF/F during the analysis range (10-min episodes, each transient or sleep state). Thus, the Z-score is specific to each analysis range, and the various Z-scores were named based on the specific range, e.g., Z-score (all stages) or Z-score (NR-R). For the calculation of Z-score (all stages), all 10-min episodes were extracted from the 24-hour recordings, which included NREM sleep (> 1 min) to REM sleep (> 1 min) transitions and wakefulness (> 1 min). Then, the Z-scores (all stages) were calculated based on the mean Z-score at each stage (Wake, NREM, REM [> 1 min] and tNR [30 sec]) of all described 10-min episodes. For the analysis of NREM sleep activity, the level of activity of orexin neurons was defined as follows: high Z-score (NR) epoch, Z-score (NR) of all the points in the epoch >1; low Z-score (NR) epoch, Z-score (NR) of all the points in the epoch <1; Mid Z-score (NR) was all other epochs. Some data in the fiber photometry experiments were excluded based on small changes in DF/F values, *post hoc* verification of viral expression, or the position of the optic fibers.

In vivo Ca^{2+} imaging using nVista

More than three weeks after AAV injection, a GRIN lens (length of 8.4 mm, diameter of 1 mm, Inscopix, Palo Alto, CA, USA) was implanted above the LHA (AP=-1.4 mm; ML=+0.9 mm; DV=-4.6 to 5.0 mm). At the same time, an acrylic bar for head fixation was attached to the skull using Super-bond (Super-bond C&B, Sun Medical, Moriyama, Japan). More than one week after implantation, the mouse was attached to a stereotaxic frame using the acrylic bar. A baseplate (Inscopix, Palo Alto, CA) was attached using dental cement (REPAIRSIN, GC) to hold a microendoscope (nVista, Inscopix). Then the microendoscope was attached to the head to monitor GCaMP6s fluorescence through the implanted GRIN lens. Images were acquired at 10-20 frames/sec with 0.2-1.1 mW of LED light (475 nm) using nVista HD Acquisition Software (version 3; Inscopix). All images were processed using Mosaic Software (version 2.0; Inscopix) and Inscopix Data Processing Software (IDPS, version 1.6.1, Inscopix). Since our

study focused on the activity of orexin neurons during sleep, in the recoding of the vigilance states (wakefulness, NREM sleep, and REM sleep; Figure 2 and 4), the mean fluorescence of all frames during NREM and REM sleep (except for wakefulness) was determined as a single reference frame (F0). Thus, F0 represented the mean fluorescence of the sleep state. In the recording of episodes with cataplexy (Figure 5 and Supplementary Figure 6), the mean fluorescence of all frames was determined as a single reference frame (F0). After image processing, single-neuron activity was separated using PCA/ICA (8) in IDPS, then synchronized with time-stamped sleep recording data at the start of each sleep-wake stage defined by the EEG/EMG signals. Synchronization accuracy of EEG/EMG recordings and Ca^{2+} imaging was estimated within 7.8 msec. The mean value (mean) and standard deviation (SD) of the GCaMP6s signal from each cell were calculated from the period of each cell showing the least activity during NREM sleep and cataplexy only in Figure 5 (due to the absence of NREM sleep in Figure 5). The “Z-score integral” was calculated by summation of the Z-score more than the mean+3 SD which was divided by the number of frames. When the Z-score integral of a neuron at a particular stage was ≥ 0.1, the neuron was classified as active at that stage. When a detected neuron was not classified as active at any stage, it was classified as a “non-classified neuron”.

To increase cataplexy frequency, chocolate (~2.1 g, milk chocolate, Meiji) was provided for at least 3 days during habituation and on the day of Ca^{2+} imaging (fiber photometry and nVista), 0-30 min(s) just prior to the dark onset (ZT12).

Clustering and correlation analysis

To examine the temporal features of orexin neuron population dynamics during NREM sleep, single episodes of NREM sleep were used for cluster analysis. Mice were selected from which more than 9 neurons could be extracted. Neurons were classified into three NREM clusters (population activity patterns) by non-negative matrix factorization (NMF, as described below) (9). To perform NMF, the negative value of the calcium signal (Z-score) was set to 0. The NREM-active cluster (pattern) was defined as cluster(s) whose intensity was above a certain threshold (maximum intensity ≥ 0.6; the value of the element of the intensity matrix) and NREM-active cluster cells were defined as cells that contributed to the formation of the NREM-active cluster above a certain threshold (contribution ≥ 1.0; the value of the element [cell] of the pattern matrix). Temporal connectivity maps of

NREM-active cluster cells were created for NREM sleep, REM sleep, and wakefulness, respectively, using the correlation coefficient (r) of the fluorescence signal between the pairs of neurons under each condition (NREM sleep, REM sleep, and wakefulness) by Pearson correlation analysis (temporal connectivity). The location of the cells was determined by the (x, y) position of the center of the neuron for the maximum projection frame in the field of view. The size of the circle representing a neuron is indicated by the percentage of links ($r \geq 0.20$) relative to all links. To clarify the connection relationship, the links were color-coded based on threshold (r=0.20) to a perfect correlation (r=1.0), thus enabling the correlation between neurons participating in synchronous activity. Finally, group means (±SEM) for the percentage of links ($r \geq 0.20$) relative to all links per cell were calculated for each condition, plotted, and statistically tested. The analysis described above, including NMF, was executed using a custom Python (3.7) script.

Non-negative matrix factorization (NMF)

Briefly, NMF finds an optimal factorization of the data matrix W so that the pattern matrix V and the corresponding intensity matrix H are as follows: $W \approx VH$ (9). The rows of W are the time series of signals from individual neurons, each column vector of V is a synchronously activated neuron ensemble (population activity pattern), and each row of H is a time series of the activation intensity of the corresponding pattern.

Optogenetic inhibition/stimulation and vigilance state-dependent illumination

Orexin-tTA mice and o*rexin-Flp (KI/KI)* mice were used for optogenetic inhibition experiments. At least three weeks after AAV injection, LED cannulae (fiber diameter 500 μm, fiber length 5 mm, bilateral, 525 nm, 3.2 mW; Bio Research Center) were implanted (AP=-1.4 mm; ML=±0.9 mm; DV=-4.5 mm) during EEG/EMG surgery. All screws, wires, and LED cannulae were secured to the connector pins using Super-Bond C&B (Sun Medical) and dental cement (GC). After a recovery period of at least 3 days, the cables for EEG/EMG and LED were connected to a slip ring (AC6023-12, Moog) designed such that the movement of the mouse was unrestricted by the cables. After 7-8 days of habituation, experiments with continuous photoillumination were conducted for 1 hour from ZT7 to ZT8, followed by a cage change. At least 3 days after the cage change,

vigilance state-dependent illumination experiments were conducted. The interval between vigilance state-dependent illumination experiments was 3-5 days. The orders of the vigilance state-dependent illumination experiments were randomized (REM-NREM-Wake-Yoked control, Yoked control-REM-NREM-Wake or REM-Yoked control-NREM-Wake [only in one *orexin-Flp* mouse]). The data obtained one day prior to each state-dependent illumination were used as the baseline.

EEG and EMG signals were amplified by an amplifier (AB-610J, Nihon Kohden), filtered (EEG, 1.5-30 Hz; EMG, 15-300 Hz), and digitized at a sampling rate of 128 Hz. EEG/EMG and locomotion signals were recorded in 4-sec epochs and spectral analysis of the EEG was performed by FFT (sampled at 128 Hz) in real time using SleepSignRecorder software (Kissei Comtec).

The vigilance state for each epoch was automatically defined in real time using the following decision tree algorithm by SleepSignRecorder: (1) locomotion detection = wakefulness; (2) high EMG integral = wakefulness; (3) high EEG delta (0.5-4.0Hz) power integral and high EEG total (0.5-30 Hz) amplitude integral = NREM sleep; (4) high EEG delta power integral and low EEG theta (6.5-9 Hz) ratio (theta power integral/total amplitude integral) = NREM sleep; (5) high EEG theta ratio and low EEG total amplitude integral = REM sleep; (6) high EEG theta ratio and low EEG delta power integral = REM sleep; 7) if criteria (1) - (6) do not apply = the same stage as previous epoch. If the algorithm detected a wake-to-REM transition, this decision was ignored and automatically scored as wake-to-wake in real time. Values for the algorithm were defined manually for each mouse by comparing offline vigilance state determinations. Photo illumination was triggered by Transistor-Transistor Logic (TTL) output from SleepSignRecorder. After the experiments, the cover ratio of illumination for each vigilance state was calculated by comparison with offline determination.

For the optogenetic stimulation experiments, LED cannulae (fiber diameter 400 μm, fiber length 5 mm, bilateral; Kyocera Corporation, Japan) were implanted (AP=-1.4 mm; ML=±0.9 mm; DV=-4.5 mm) into the bigenic mice (*orexin-tTA; TetO channelrhodopsin2 [ChR2]*) during EEG/EMG surgery. After a recovery period of at least 3 days and at least 7 days of habituation, experiments with intermittent photoillumination (475 nm, 6.0 mW, 20 Hz for 8 sec, 4 times/minute) were conducted for 1 hour from ZT6 to ZT7.

Data from one *orexin-tTA* mouse in the optogenetic inhibition experiments were excluded based on *post hoc* verification of the position of the optic fiber.

Other data were excluded due to noisy EEG which precluded accurate determination of vigilance states in the continuous 1-hour photoillumination experiment and occasional noisy EMG which prevented correct vigilance state-dependent illumination in one *orexin-tTA* mouse, respectively. In one *orexin-tTA* mouse, the coverage of REM sleep state-dependent illumination was extremely low, particularly in the latter part of the illumination period (in this instance, REM sleep increased in the latter part of the illumination period compared to baseline). In this case, we reconducted the REM sleep state-dependent illumination after the other vigilance state-dependent illumination experiments and used the data from the second REM sleep state-dependent illumination. Three *orexin-Flp (KI/KI)* mice did not show cataplexy during any of the experiments, in these cases, we excluded the data from these 3 mice. In the intermittent optogenetic stimulation experiment, the data of one mouse which had no REM sleep at baseline was excluded.

Electrophysiology with optogenetics using brain slice preparations

Male and female mice (10-24 weeks) were used for the electrophysiological experiments. At least 3 weeks after stereotaxic AAV injection, mice were deeply anesthetized using isoflurane (Fujifilm Wako Pure Chemical Corporation) and decapitated. Brains were rapidly isolated and chilled in ice-cold bubbled (95% O_2 and 5% CO_2) cutting solution (in mM: 110 K-Gluconate, 15 KCl, 0.05 EGTA, 5 HEPES, 26.2 $NaHCO_3$, 25 Glucose, 3.3 $MgCl_2$, 0.0015 3-((+/-)-2-Carboxypiperazin-4-yl)-Propyl-1-Phosphonic acid (CPP)). Coronal brain sections of 300-μm thickness were made using a vibratome (VT-1200S, Leica). The slices were incubated in a bubbled (95% O_2 and 5% CO_2) bath solution (in mM: 124 NaCl, 3 KCl, 2 $MgCl_2$, 2 $CaCl_2$, 1.23 $NaH_2PO_4.2H_2O$, 26 $NaHCO_3$, 25 glucose) at 35°C for 30 min following another 30 min incubation at room temperature in the same solution. After the incubation period, the brain slices were placed in a recording chamber (RC-26G, Warner Instruments, Hamden, CT) which was perfused at a rate of 1.5 ml/min using a peristaltic pump (Miniplus3, Gilson, USA) and bubbled with 95% O_2 and 5% CO_2. An infrared camera (C3077-78, Hamamatsu Photonics, Hamamatsu, Japan) was installed on an upright fluorescence microscope (BX51WI, Olympus, Tokyo, Japan) together with an electron multiplying charge-coupled device camera (Evolve 512 delta, Photometrics, Tucson, AZ) and monitors visualized both images separately. Glass micropipettes were prepared from borosilicate glass capillaries (GC150-10,

Harvard Apparatus, Cambridge, MA) using a horizontal puller (P1000 Sutter Instrument, Novato, CA) maintaining a pipette resistance of 4-8 MΩ. Patch pipettes were filled with KCl-based internal solution (in mM: 145 KCl, 1 $MgCl_2$, 10 HEPES, 1.1 EGTA, 2 Mg-ATP, 0.5 Na_2-GTP; pH 7.3 with KOH) with osmolality between 280-290 mOsm. After confirming that the orexin neurons expressed either GCaMP6s, ArchT or ChR2, the pipette was moved toward the cell and a positive pressure was applied manually in the patch pipette. The pressure was released when the tip of the pipette touched the cell membrane and a gigaseal was formed. The patch membrane was then ruptured by briefly applying strong suction to form a whole-cell configuration. During recording, electrophysiological properties of the cells were continuously monitored using the Axopatch 200B amplifier (Axon Instruments, Molecular Devices, Sunnyvale, CA). For the cessation of spontaneous firing in the calcium imaging experiment, the recorded neuron was hyperpolarized by applying negative current injection of -60 to -80 pA through an amplifier. To induce an action potential, ~50 pA depolarizing rectangular current (2 ms width) was applied through the recording pipette at frequencies of 5, 10, 20, or 50 Hz for 10 sec using an electric stimulator (SEN-7203; Nihon Kohden, Japan). Output signals were low pass filtered at 5 kHz and digitized at a 10 kHz sampling rate. Patch clamp data were recorded using an analog-to-digital (AD) converter (Digidata 1550A, Molecular Devices) and pClamp 10.7 software (Molecular Devices). Green light of 549 ± 7.5 nm wavelength was generated by a light-emitting diode (LED) light source (Spectra light engine, Lumencor, USA) that was directed to the microscope stage with a 1.0 cm diameter optic fiber. Coronal brain slices were illuminated through the objective lens of the fluorescence microscope. For ArchT-expressing orexin neuron recordings, green light of 0.01 mW (1%) to 4.06 mW (100%) was used.

Electrophysiology recordings with calcium imaging using brain slice preparations

An LED light source (Spectra light engine, Lumencor, Beaverton, USA) was used for excitation of GCaMP6s emission. Brain slices containing the LHA were illuminated with blue light of 475 ± 17.5 nm wavelength (3.19 mW) through the objective lens of a fluorescence microscope. GCaMP6s fluorescence intensity was recorded using MetaMorph software (Molecular Devices, Sunnyvale, CA, USA) at a rate of 2 Hz with 100 msec of exposure time. To synchronize the calcium imaging and patch clamp recordings, pClamp software was triggered by the TTL output from MetaMorph software. MetaMorph data were analyzed by

drawing a region of interest (ROI) on GCaMP6s-expressing orexin neurons and the DF/F was calculated from the average intensity of the ROI.

Immunohistochemical study

Under deep anesthesia with mixed anesthetic agents (medetomidine, midazolam, and butorphanol), mice were subject to transcardial perfusion with about 25 ml of chilled saline, followed by about 25 ml of chilled 10% formalin solution (Wako Pure Chemical Industries). The brain was gently collected, then post-fixed in 10% formalin solution at 4°C overnight. Brains were then immersed in 30% sucrose in phosphate-buffered saline (PBS) at 4°C for at least 2 days. Brains were placed into O.C.T. compound (Sakura Finetek Japan) and frozen at -80°C for at least 20 min then placed into a -20°C cryostat (Leica CM3050S; Leica Microsystems, Wetzlar, Germany). A series of coronal brain slices of 40 μm thickness was obtained with the cryostat. For staining, a series consisting of every 4th section (40 μm) was immersed in blocking buffer (1% bovine serum albumin [BSA] and 0.25% Triton-X in PBS) and incubated with primary antibodies at 4°C overnight. The sections were washed with blocking buffer and then incubated with secondary antibodies for 1-4 hour(s) at room temperature or 4°C overnight. The brain sections were mounted and examined with a fluorescence microscope (BZ-X710, Keyence, Osaka, Japan) and analyzed with ImageJ (US National Institutes of Health). Primary and secondary antibodies were diluted in blocking buffer as follows: anti-orexin-A rabbit antibody (Phoenix Pharmaceuticals, Burlingame, CA, USA) at 1:2000; anti-MCH rabbit antibody (Sigma-Aldrich, Tokyo, Japan) at 1:1000; CF 594-conjugated anti-rabbit antibody (Biotium Inc., Hayward, CA, USA) at 1:2000 (Orexin-A) or 1:1000 (MCH). For manual cell counting, a series consisting of every 4th brain section containing the LHA was examined with Image J.

Statistical analysis

Statistical analyses were performed using OriginPro 2020 software (LightStone, Tokyo, Japan), easy R (1.37), or Python (3.7). All data are presented as the mean ± SEM. Details of the statistical tests are described in Supplementary Table 1. Significant differences were set at $P<0.05$.

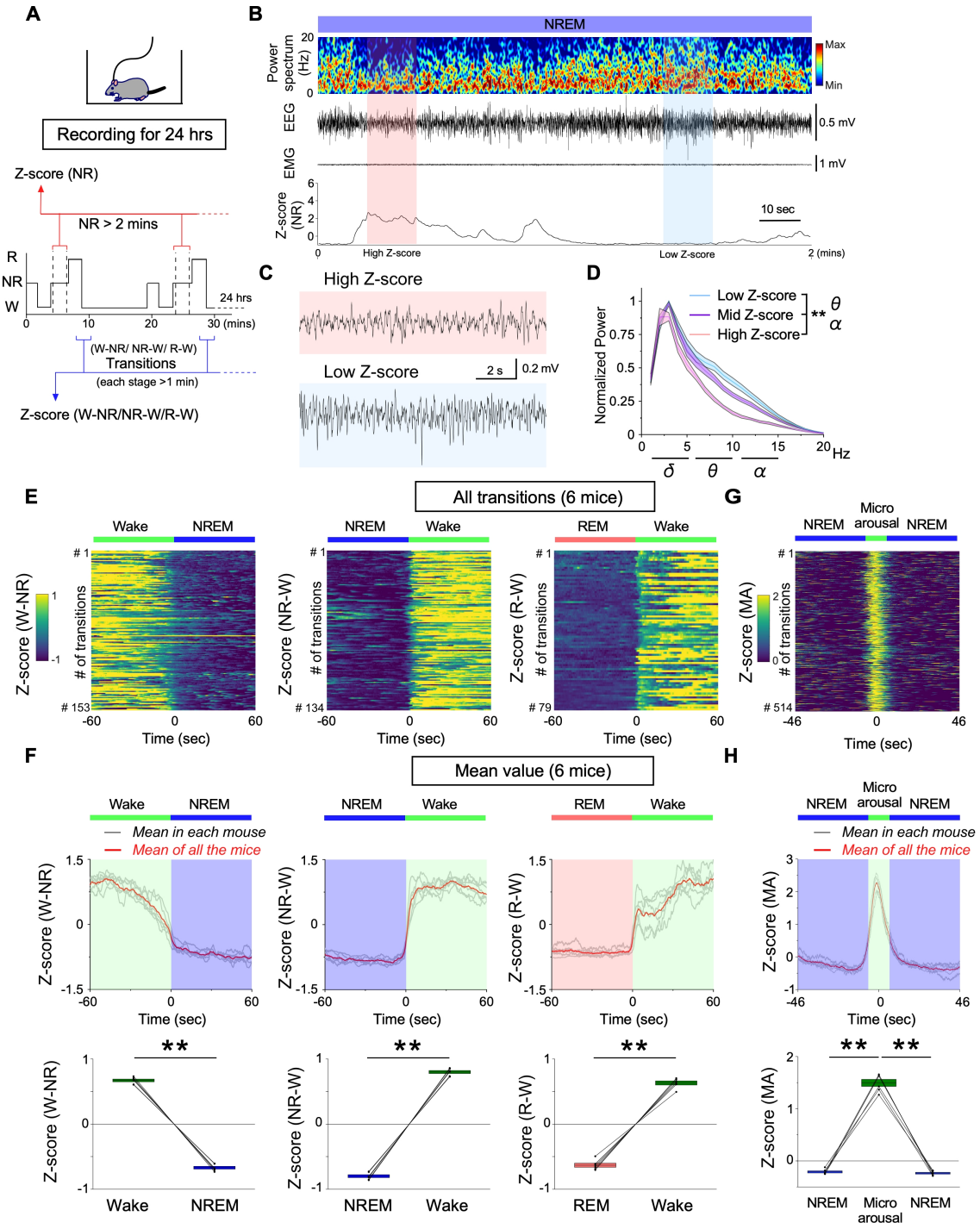

Supplementary Figure 1. Fiber photometry recordings of orexin neurons activity across vigilance states and during NREM sleep in *orexin-tTA* mice. (A) Schematics of experimental procedures and data analysis. (B) Representative orexin neuronal activity during NREM sleep measured by fiber photometry. (C) Enlargement of the EEG in (B) for the epochs when the activity of orexin neurons was low (low Z-score (NR)) and high (high Z-score (NR)) during

NREM sleep. (D) EEG spectrum in NREM sleep epochs with Low, Mid and High Z-scores (NR). (E) Activity of orexin neurons in all transitions between states (each stage > 1 min). (F) (top) Mean of all mice (red) and mean of all the transitions in individual mice (gray). (bottom) Summary of activity during state transitions. (G) Activity of orexin neurons in all measured microarousals (defined as wakefulness < 12 sec, flanked by NREM sleep > 40 sec). (H) (top) Mean of all mice (red) and mean of individual mice (gray). (bottom) Summary of activity during microarousal. Values represent the mean ± SEM. * $P < 0.05$, ** $P < 0.01$. Statistical analyses are shown in Supplementary Table 1. W, wakefulness; NR, NREM; R, REM; MA, microarousal.

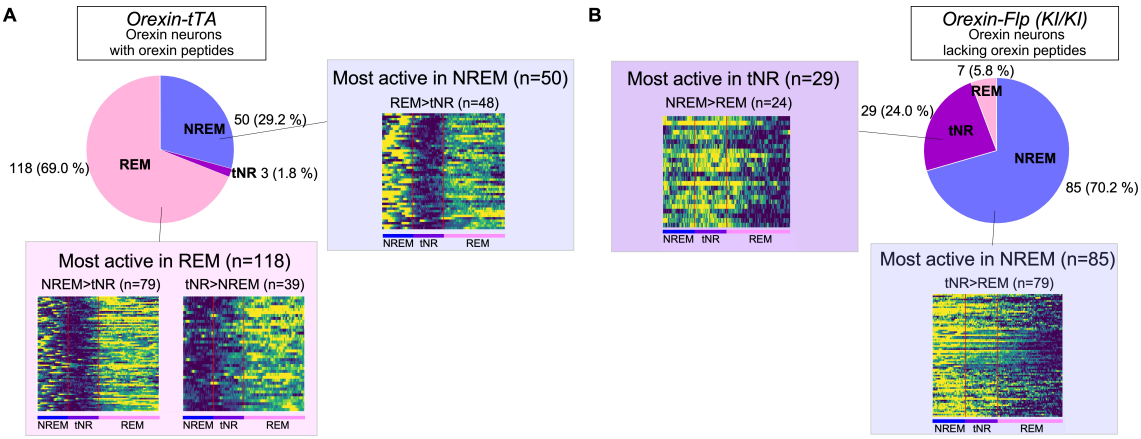

Supplementary Figure 2. Absence of the orexin peptides disrupts the activity dynamics of orexin neurons during transitions from NREM sleep to REM sleep.

Based on fiber photometry recordings, NREM-REM transitions in *orexin-tTA* (A) and *orexin-Flp (KI/KI)* (B) mice were classified according to the vigilance state (NREM, REM or tNR) during which orexin neuron activity was the highest. Pie charts show the proportion of vigilance states in which the highest orexin neuron activity occurred in 171 transitions in *orexin-tTA* mice and 121 transitions in *orexin-Flp (KI/KI)* mice. Whereas orexin neuron activity was greatest during REM sleep in 69.0% of the transitions in *orexin-tTA* mice, in the absence of the orexin peptides, that proportion was only 5.8% in *orexin-Flp (KI/KI)* mice.

In detail, a reduction of activity prior to transition to REM sleep and higher activity during REM sleep occurred in almost every transition (97.1%; 166 [48 (NREM>REM>tNR) + 118 (most active in REM)] of 171 transitions) in *orexin-tTA* mice that expresses the orexin peptides. In contrast, in the absence of the orexin peptides in *orexin-Flp (KI/KI)* mice, the lowest activity during REM sleep was observed in most of the transitions (85.1%; 103 [24 (tNR>NREM>REM) + 79 (NREM>tNR>REM)] of 121 transitions) and the highest orexin neuron activity was observed during the tNR in 24.0% (29 transitions). tNR, last 30 sec during the transition from NREM to REM sleep; NR, NREM; R, REM.

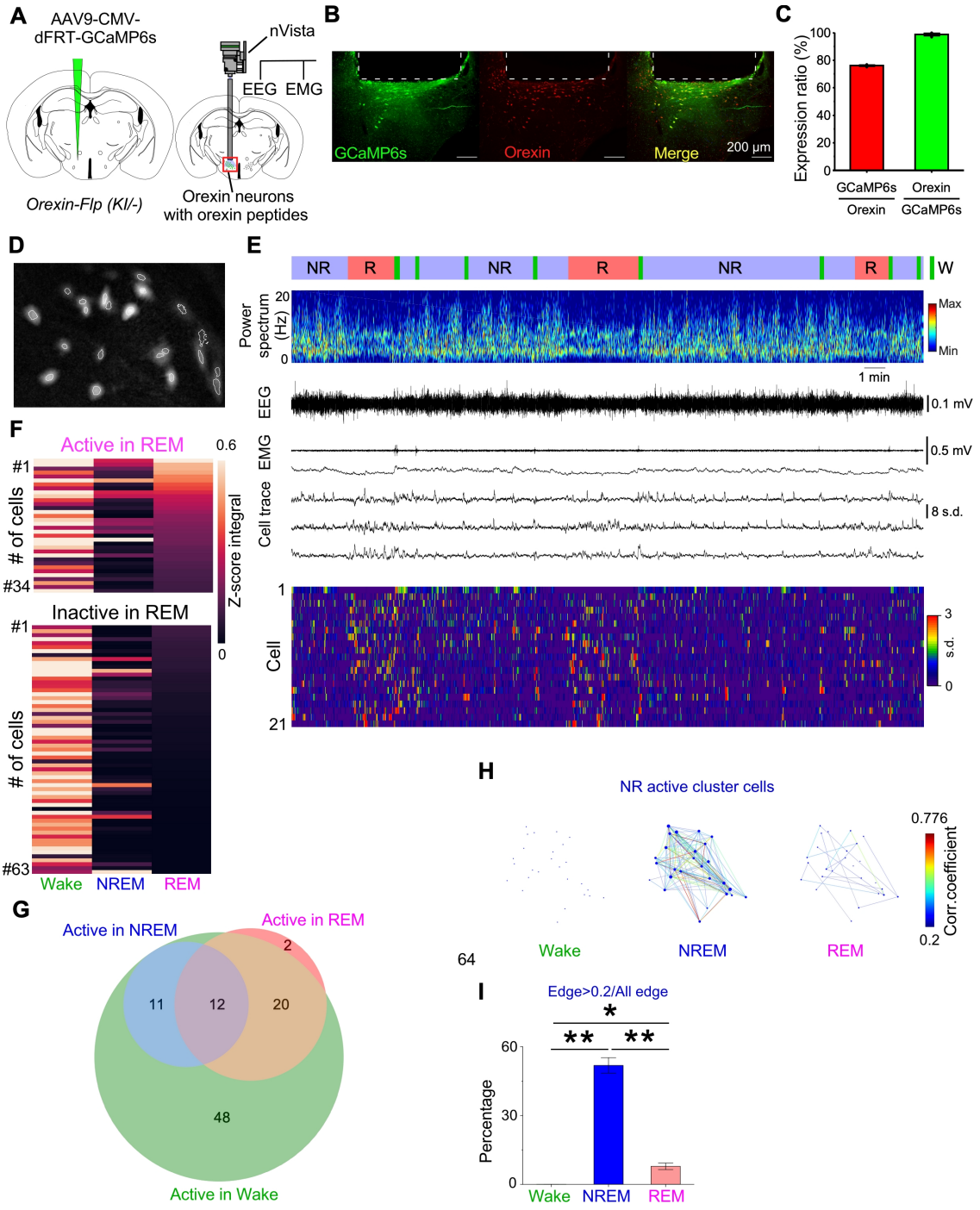

Supplementary Figure 3. Activity recordings of orexin neurons that express orexin peptides across vigilance states in *orexin-Flp (KI/-)* mice as determined by microendoscopy.

(A) Schematics of GCaMP6s expression (left) and microendoscopy (nVista) with EEG and EMG recordings (right). (B) Immunohistochemical confirmation of GCaMP6s expression in orexin neurons. The dashed lines indicate trace of GRIN lens. (C) Quantitative cell counts showing GCaMP6s expression exclusively in

orexin neurons in 3 mice. (D) Representative identification of orexin neurons using nVista. Dashed white line indicates region of interest (ROI). (E) Representative traces of EEG, EMG, and Ca^{2+} activity during each vigilance state. (F) Activity of REM-active and -inactive orexin neurons during each vigilance state. (G) Venn diagram showing the proportion of the 93 orexin neurons (3 mice) exhibiting each activity pattern. A total of 98 cells were detected; 5 neurons were not classified to a particular state. (H) Representative activity correlations among neuronal pairs from all NREM-active clusters. (I) Percentage of activity synchronization (proportion of correlated pairs, >0.2) at each vigilance state. Data are the mean ± SEM. *P < 0.05, **P < 0.01. Statistical analyses are shown in Supplementary Table 1. W, wakefulness; NR, NREM; R, REM.

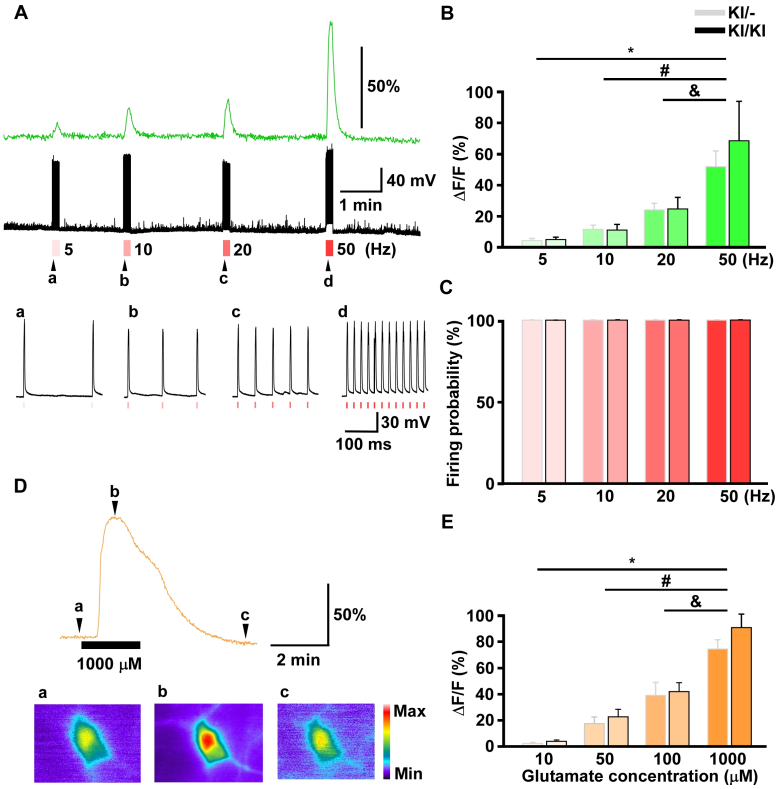

Supplementary Figure 4. In vitro confirmation of GCaMP6s signal in *orexin-Flp (KI/-) and orexin-Flp (KI/KI)* mice.

(A) Representative traces from an orexin knockout (*orexin-Flp (KI/KI))* mouse showing the correlation between calcium signals and induced firing frequency. The upper trace shows the fluorescence intensity, and the lower trace shows the membrane potential. Positive-current injection through the recording pipette induced (a) 5 Hz, (b) 10 Hz, (c) 20 Hz, and (d) 50 Hz firings. Timing of the current injections are indicated by the red bars. Arrowheads indicate the position of the magnified traces (a, b, c, and d) in the lower panel. (B, C) Summary of (A). ΔF/F (B) and firing probability (C) recordings from *orexin-Flp (KI/-)* mice (gray bar, n=3 mouse; n=8 cells) and *orexin-Flp (KI/KI)* mice (black bar, n=3 mouse; n=6 cells). *, 5 Hz vs 50 Hz (KI/-: P = 4.7 x 10^{-06}; KI/KI: P = 0.0094), #, 10 Hz vs 50 Hz (KI/-: P = 0.000048; KI/KI: P = 0.019), &, 20 Hz vs 50 Hz (KI/-: P = 0.0035; KI/KI: P = 0.11). (D) Glutamate-induced activation of orexin neurons in *orexin-Flp (KI/-)* and *(KI/KI)* mice. The upper trace represents fluorescence intensity after application of glutamate (1000 μM) and the lower panel shows pseudo-colored images of fluorescence intensity at different time points indicated by the arrowheads labeled a, b, and c. (E) Summary of (D) recordings from *orexin-Flp (KI/-)* mice (gray bar, n=3 mouse; n=9 cells) and o*rexin-Flp (KI/KI)* mice (black

bar, n=3 mouse; n=11 cell). *, 10 μM vs 1000 μM (KI/-: P = 1.0 x 10^{-9}; KI/KI: P = 1.1 x 10^{-12}), #, 50 μM vs 1000 μM (KI/-: P = 9.4 x 10^{-8}; KI/KI: P = 3.9 x 10^{-10}), &, 100 μM vs 1000 μM (KI/-: P = 0.00018; KI/KI: P = 4.7 x 10^{-07}). Data are the mean ± SEM. Statistical analyses were made by one-way ANOVA repeated measurement (RM), and Bonferroni's multiple comparison test.

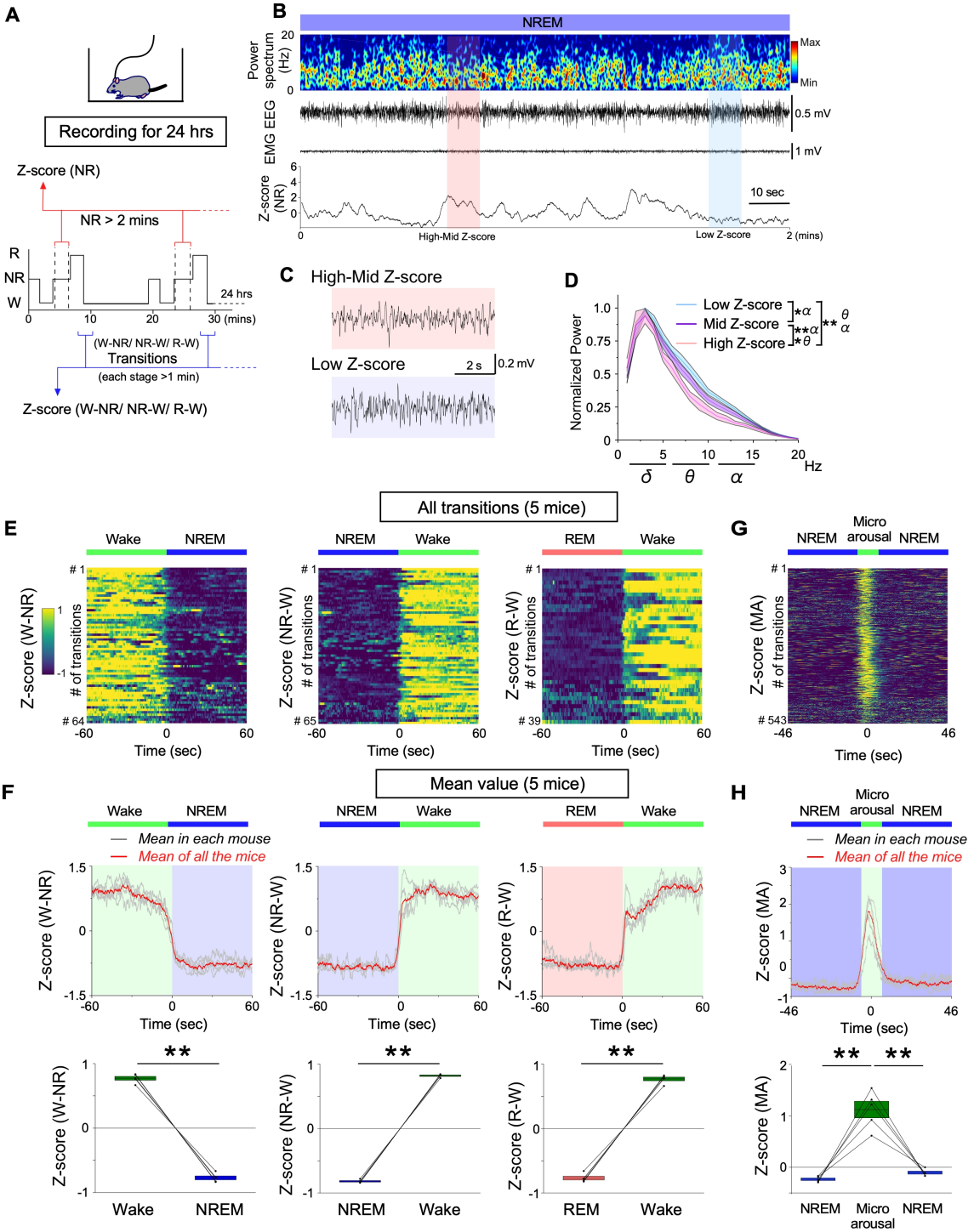

Supplementary Figure 5. Fiber photometry recordings of orexin neuron activity across vigilance states and during NREM sleep in *orexin-Flp (KI/KI)* mice that do not synthesize the orexin peptides.

(A) Schematics of experimental procedures and data analysis. (B) Representative orexin neuronal activity during NREM sleep measured by fiber photometry. (C) Enlargement of the EEG in (B) for the epochs when the activity

of orexin neurons was low (low Z-score (NR)) and high (high-mid Z-score (NR)) during NREM sleep. (D) EEG spectrum in NREM sleep epochs with low, mid and high Z-scores (NR). (E) Activity of orexin neurons in all the transitions between states (each stage > 1 min). (F) (top) Mean of all mice (red) and mean of all the transitions in individual mice (gray). (bottom) Summary of activity during state transitions. (G) Activity of orexin neurons in all measured microarousals (defined as wakefulness < 12 sec, flanked by NREM sleep > 40 sec). (H) (top) Mean of all mice (red) and mean of individual mice (gray). (bottom) Summary of activity during microarousal. Values are the mean ± SEM. *P < 0.05, **P < 0.01. Statistical analyses are shown in Supplementary Table 1. W, wakefulness; NR, NREM; R, REM; MA, microarousal.

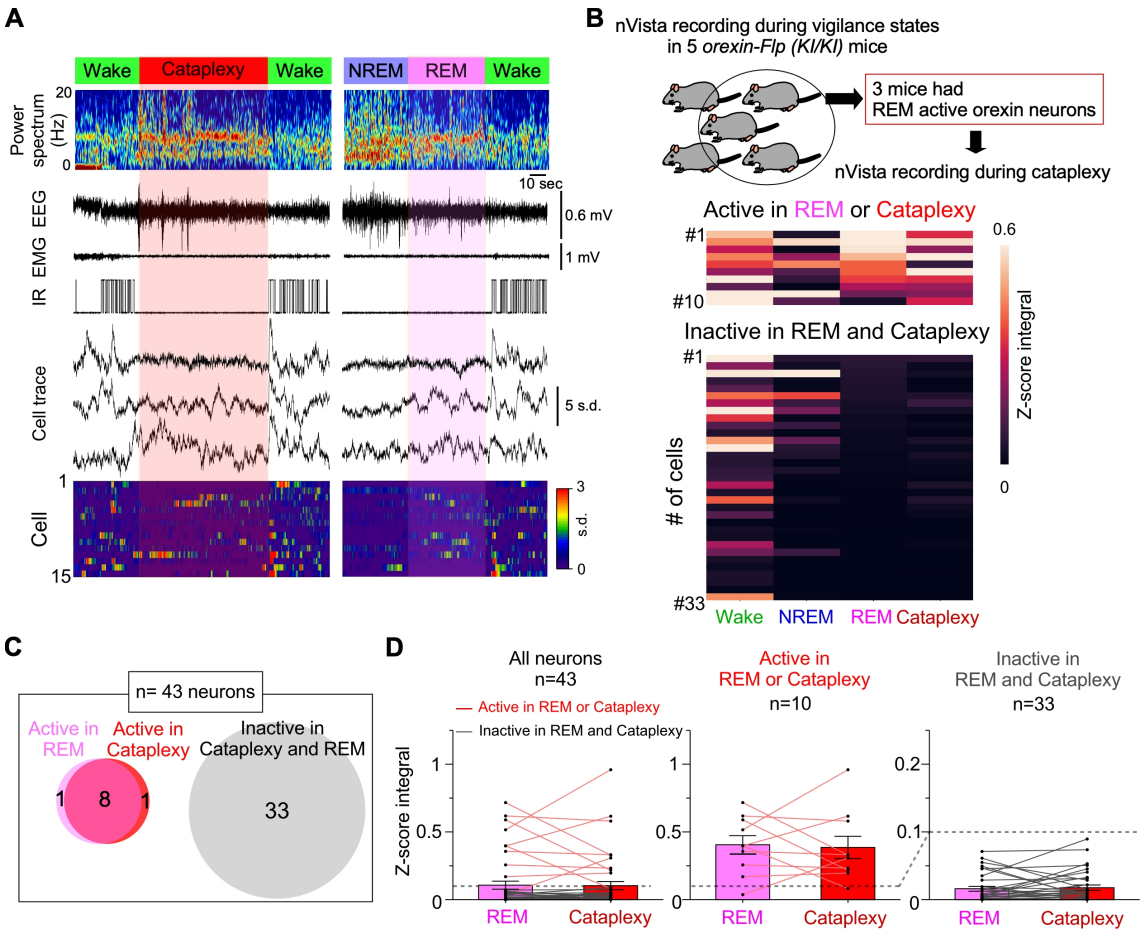

Supplementary Figure 6. Activity of orexin neurons during cataplexy and REM sleep in *prepro-orexin* knockout (*orexin-Flp (KI/KI)*) mice.

(A) Representative traces of EEG, EMG, and Ca^{2+} activity during each vigilance state. (B) For the technical difficulty of recording cataplexy and REM sleep, we could record the activity during cataplexy only in three *orexin-Flp (KI/KI)* mice which had REM-active orexin neurons. Heatmap shows activity of REM-active and -inactive orexin neurons during each vigilance state. In the three mice which have REM-active orexin neurons, 79.1% (34 out of 43 neurons) of orexin neurons in *orexin-Flp (KI/KI)* mice were silent during cataplexy. The duration of the recording period for REM sleep and cataplexy were 71 ± 23 sec, and 153 ± 51 sec. The number of bouts of REM sleep and cataplexy is one episode for each mouse. The number of ROIs in three mice was 16, 15 and 12 neurons, respectively (C) Venn diagram showing the proportion of the 10 orexin neurons (n=3 mice) exhibiting activity during REM sleep or cataplexy, as well as the 33 inactive orexin neurons during REM sleep and cataplexy. (D) Z-score integral of orexin neurons which are active during REM sleep or cataplexy, as well as

inactive during REM sleep and cataplexy. Data are the mean ± SEM. Statistical analyses are shown in Supplementary Table 1. Wake, wakefulness. IR, infrared sensor.

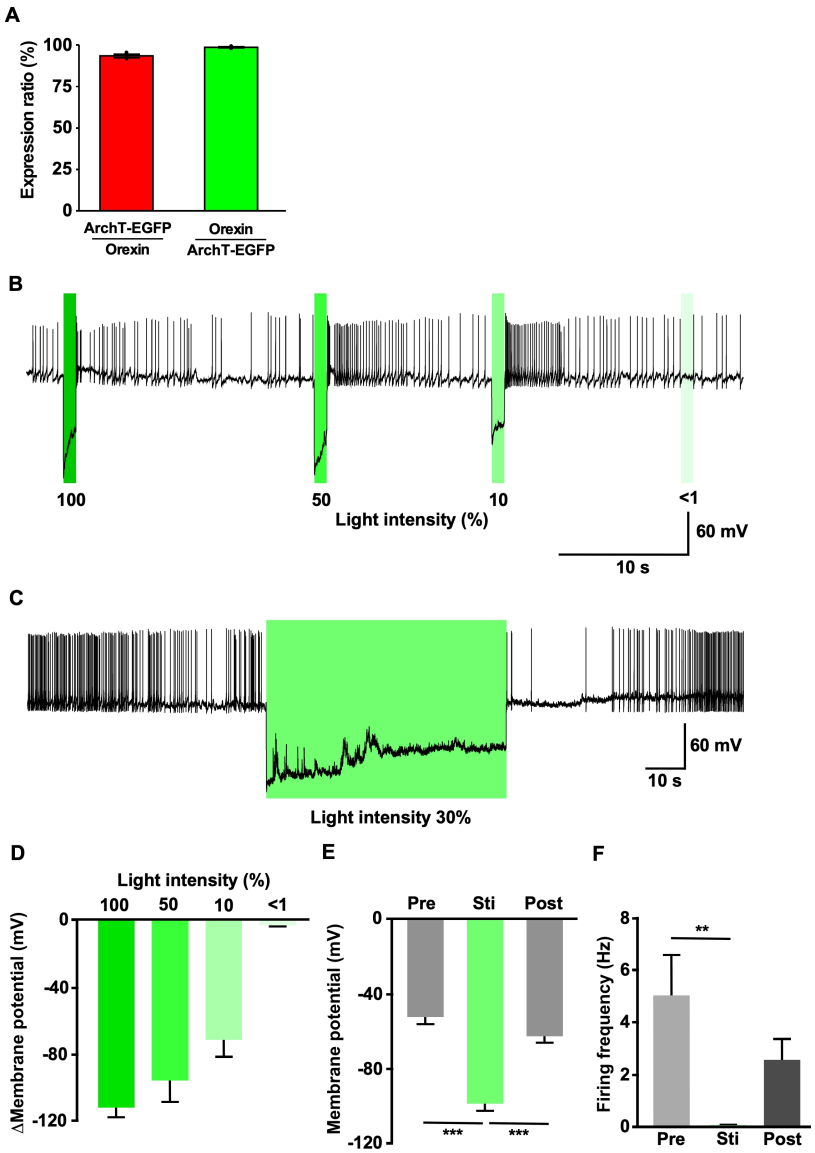

Supplementary Figure 7. *In vitro* confirmation of ArchT expression and function in o*rexin-tTA* mice.

(A) Quantitative cell counts showing ArchT-EGFP expression exclusively in orexin neurons in 3 mice. (B) Representative trace from a current clamp recording from ArchT-EGFP-expressing orexin neurons. Green light (549 ± 7.5 nm) of different intensities induced hyperpolarization in green light intensity-dependent manner. (C) Continuous green light illumination for 1 min with 30% intensity (1.53 mW) inhibited firing. (D) Summary of (B) (n=3 mice; n=12 cells). (E and F) Summary of membrane potential (E) and firing rate (F) from (C) (n=3 mice; n=12 cells). Data are the mean ± SEM. All statistical analyses were one-way ANOVA repeated measurement (RM), and Bonferroni's multiple comparison test. * P < 0.05, **P < 0.01 and ***P <0.001.

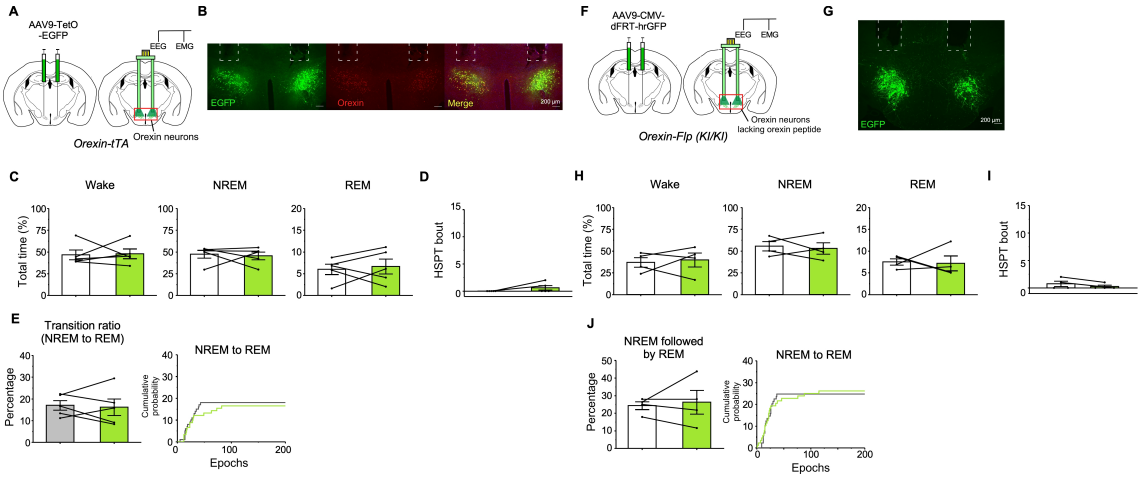

Supplementary Figure 8. Effects of photoillumination of orexin neurons on vigilance state transitions in *orexin-tTA* and *orexin-Flp (KI/KI)* mice expressing EGFP or GFP rather than ArchT-EGFP.

(A) Schematics of EGFP expression in orexin neurons that expressed orexin peptides in *orexin-tTA* mice (left) and implantation of bilateral fiber optics with EEG/EMG recordings (right). (B) Immunohistochemical confirmation of EGFP expression in orexin neurons of *orexin-tTA* mice. Dashed lines indicate the location of the optic fibers. (C) Total time in each vigilance state during baseline (gray) and photoillumination (green). (D) Number of HSPT bouts during baseline (gray) and photoillumination (green) of orexin neurons in *orexin-tTA* mice. (E) Transition ratio (left) and cumulative probability (right) for the NREM to REM sleep transition. (F) Schematics of hrGFP expression in orexin neurons from *orexin-Flp (KI/KI)* mice that lack orexin peptides (left) and implantation of bilateral optical fibers along with EEG/EMG recordings (right). (G) Histochemical confirmation of GFP expression in *orexin-Flp (KI/KI)* mice; dashed lines indicate location of the optical fibers. (H) Total time in each vigilance state during baseline (gray) and during photoillumination (green). (I) Number of HSPT bouts during baseline (gray) and photoillumination (green) of orexin neurons in *orexin-Flp (KI/KI)* mice. (J) Transition ratio (left) and cumulative probability (right) for the transition between NREM to REM sleep. Values are the mean ± SEM. Statistical analyses are shown in Supplementary Table 1. HSPT, hypersynchronous paroxysmal theta burst.

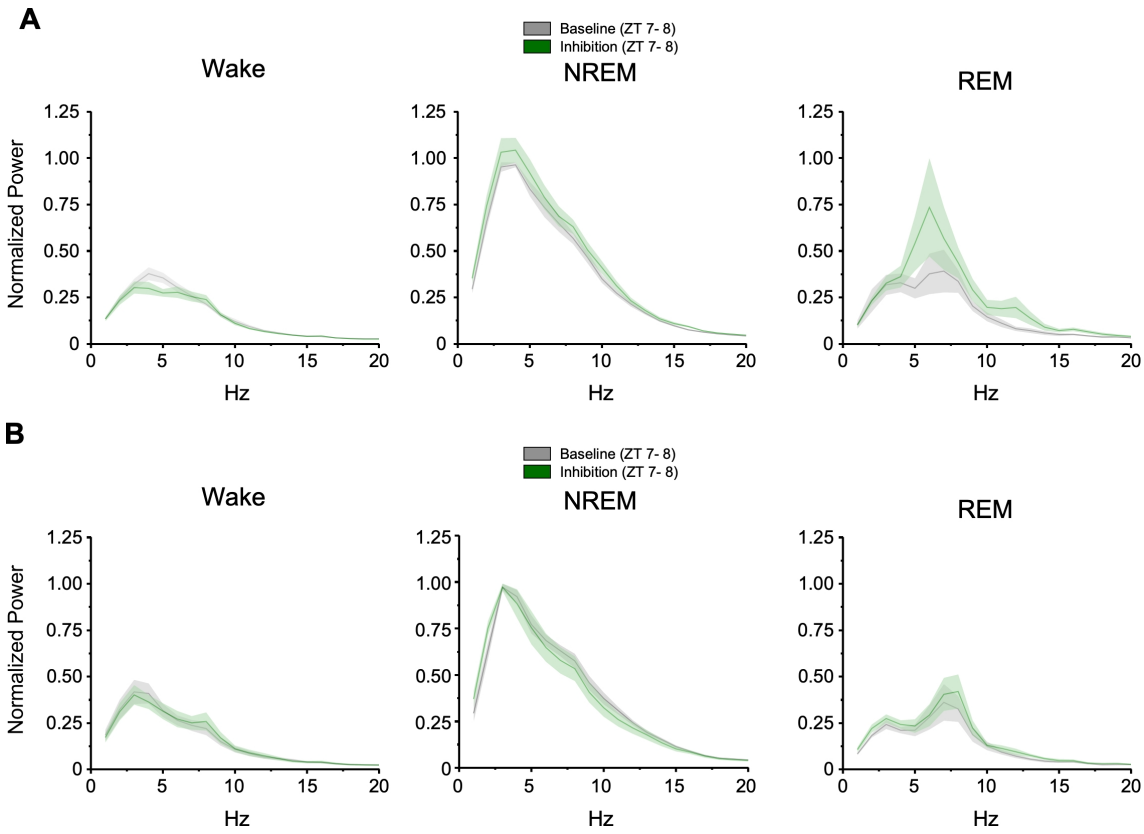

Supplementary Figure 9. Effect of optogenetic inhibition of orexin neurons with and without orexin peptides on EEG spectra.

(A) Effects of optogenetic inhibition of orexin neurons for 1 hour on EEG spectra in *orexin-tTA* mice (6 mice) which synthesize the orexin peptides. (B) Effects on EEG spectra in *orexin-Flp (KI/KI)* mice (6 mice), a strain in which the orexin peptides are not synthesized. Values are the mean ± SEM. Statistical analyses are shown in Supplementary Table 1.

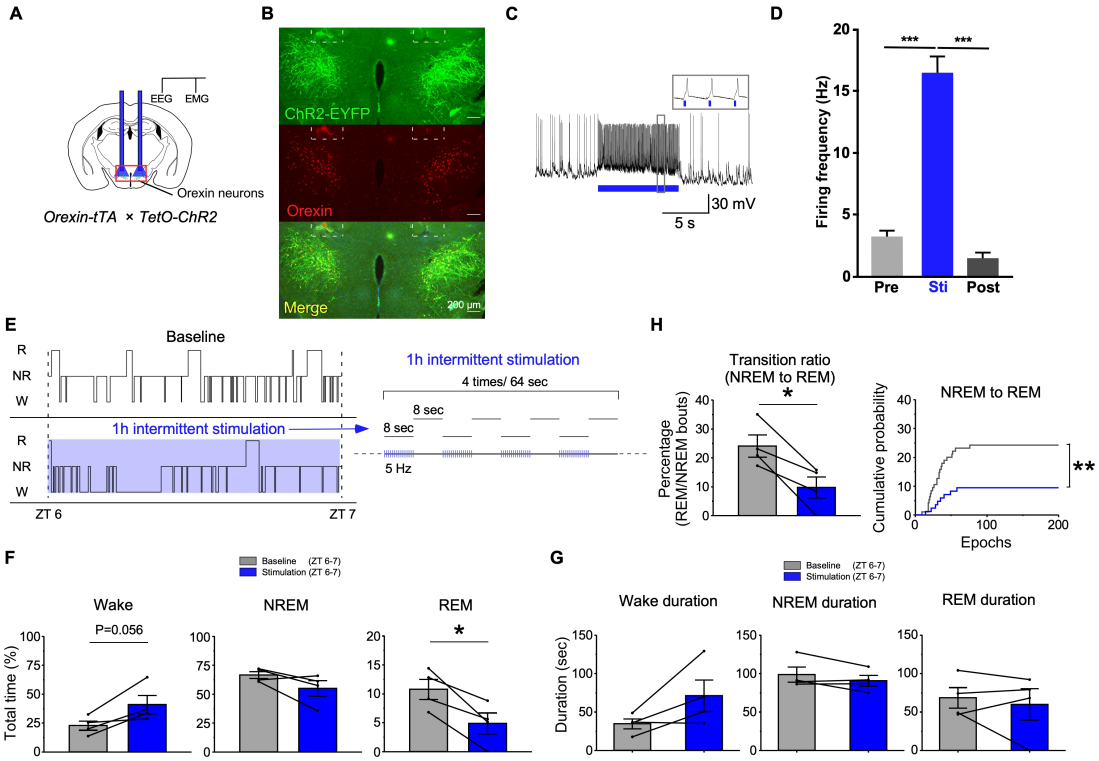

Supplementary Figure 10. Effects of intermittent optogenetic stimulation of orexin neurons on transitions from NREM sleep to REM sleep in bigenic *orexin-tTA; TetO-ChR2* mice.

(A) Schematics of ChR2 expression and optical fiber insertion using bigenic *orexin-tTA; TetO-ChR2* mice. (B) Immunohistochemical confirmation of ChR2 expression in orexin neurons. (C) Representative trace of a current clamp recording from ChR2-EYFP-expressing orexin neurons. Blue bar indicates blue light (475 ± 17.5 nm, 20 Hz, 5 ms pulse for 8 sec, 50% intensity (3.19 mW)) induced depolarization. Inset shows pulse-generated action potentials. (D) Summary of (C) (n=3 mice; n=12 cells). Data are the mean ± SEM. The statistical analysis was one-way ANOVA repeated measurement, and Bonferroni's multiple comparison test. ***P <0.001. (E) Representative hypnogram (ZT6-7) during baseline (upper left) and intermittent optogenetic stimulation (lower left). Schematics showing intermittent (4 times/~1 min) photoillumination protocols (right). (F and G) Total time and duration in each vigilance state at baseline (gray) and during optogenetic inhibition (blue). Here, a duration with no episodes of REM sleep is represented as 0. (H) Transition ratio (left) and cumulative probability (right) for the NREM to REM sleep transition. Values are the mean ± SEM. *P < 0.05, **P < 0.01. Statistical analyses are shown in Supplementary Table 1.

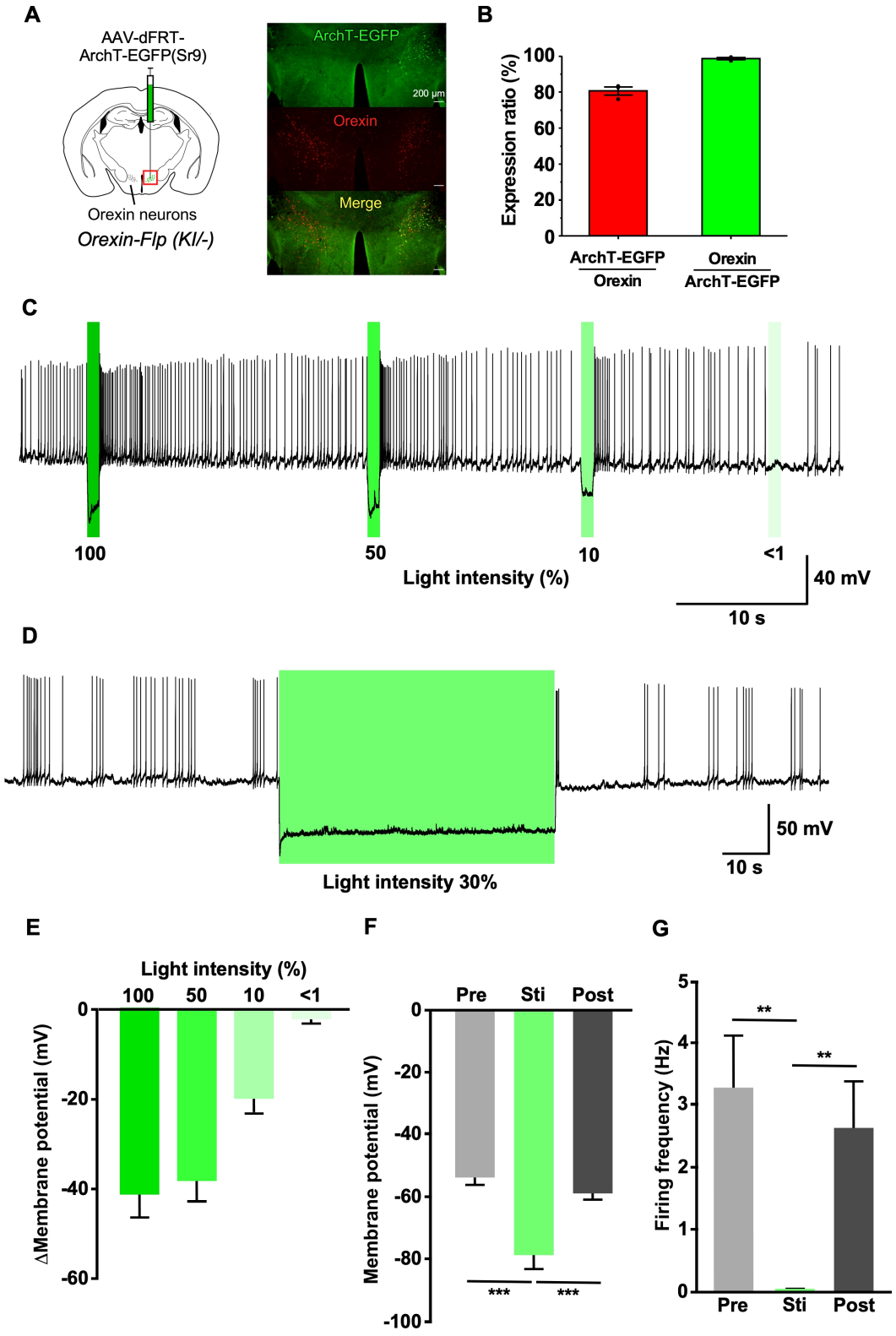

Supplementary Figure 11. Confirmation of ArchT expression and function in orexin neurons in *orexin-Flp* mice.

(A) Schematic of ArchT expression using *orexin-Flp (KI/-) mice* (left) and

immunohistochemical confirmation (right). (B) Quantitative cell counts showing ArchT expression exclusively in orexin neurons in 3 mice. (C) Representative trace from a current clamp recording from ArchT-EGFP-expressing orexin neurons lacking orexin peptides (from *orexin-Flp (KI/KI)* mice). Green light (549 ± 7.5 nm) induced hyperpolarization in an intensity-dependent manner. (D) Continuous green light stimulation for 1 min with 30% intensity (1.53 mW) inhibited firing. (E) Summary of data from (C) (n=3 mice; n=10 cells). (F and G) Summary of membrane potential (F) and firing rate (G) from (D) (n=3 mice; n=10 cells). Values are the mean ± SEM. All statistical analyses were one-way ANOVA repeated measurement (RM), and Bonferroni's multiple comparison test. **P < 0.01, and ***P <0.001.

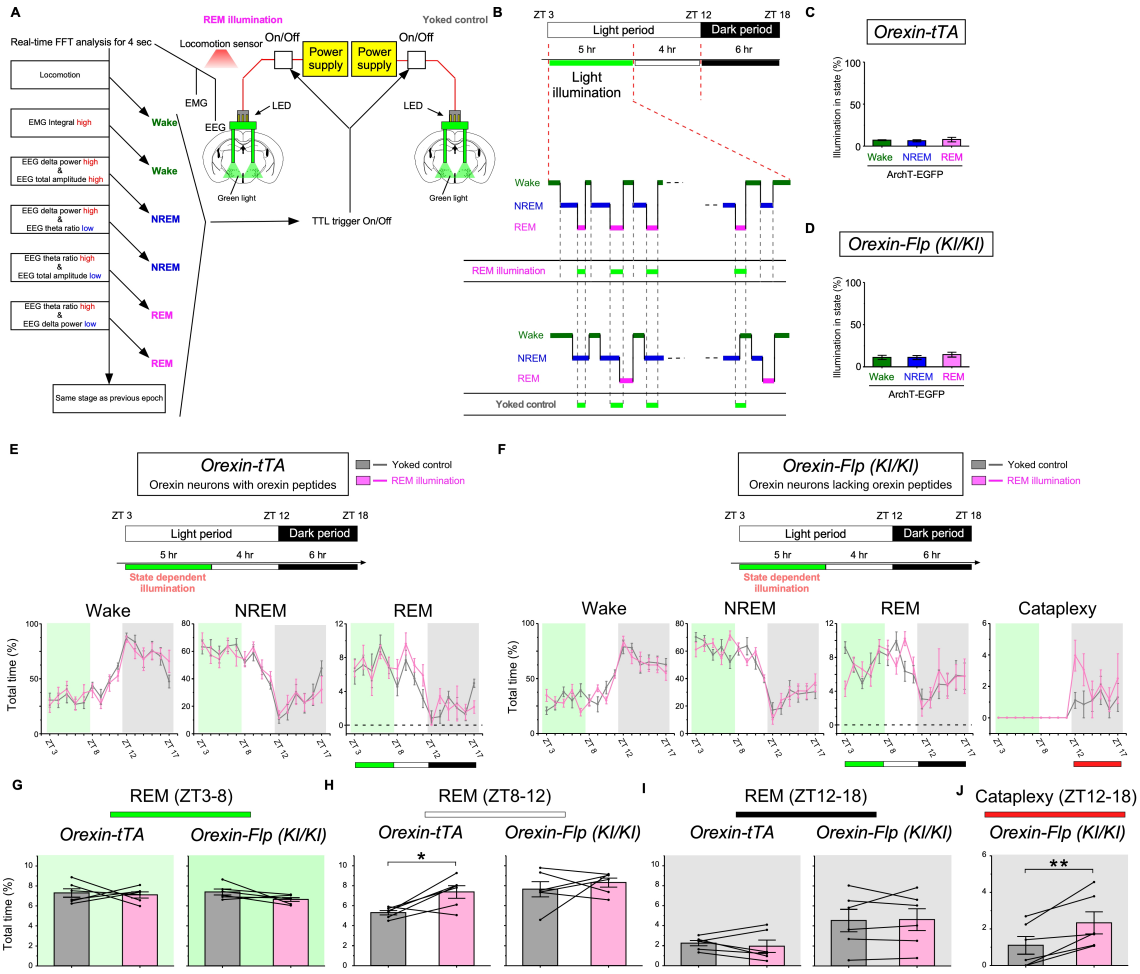

Supplementary Figure 12. REM sleep state-dependent inhibition of orexin neurons with and without orexin peptides in experimental and yoked control mice.

The data from REM sleep state-dependent inhibition are the same as the data depicted in Figure 7 but compared with yoked controls. (A) Decision tree algorithm of real-time vigilance state discrimination using EEG, EMG, and locomotion for photoillumination of experimental and yoked control mice. Yoked control mice received photoillumination whenever a paired mouse showed REM sleep. (B) Schematic showing an example of state-dependent illumination with a yoked control. (C and D) Bar graphs indicating the percentage of illumination time in each state in yoked control *orexin-tTA* mice (C) and orexin knockout (*orexin-Flp (KI/KI)*) mice (D). (E-J) Effect of REM sleep state-dependent illumination on total time in each vigilance state during state-dependent illumination (ZT3-8), during the subsequent light period (ZT8-12), and during the subsequent dark period (ZT12-18) in *orexin-tTA* mice (E and left panels in G-I) and orexin knockout

(*orexin-Flp (KI/KI)*) mice (F and right panels in G-I and J) compared to yoked control mice. The statistical results from other vigilance states at each time period are described in Supplementary Table 1. Data are the mean ± SEM. *P < 0.05, **P < 0.01. Statistical analyses are shown in Supplementary Table 1. FFT, fast Fourier transform; TTL, transistor-transistor logic.

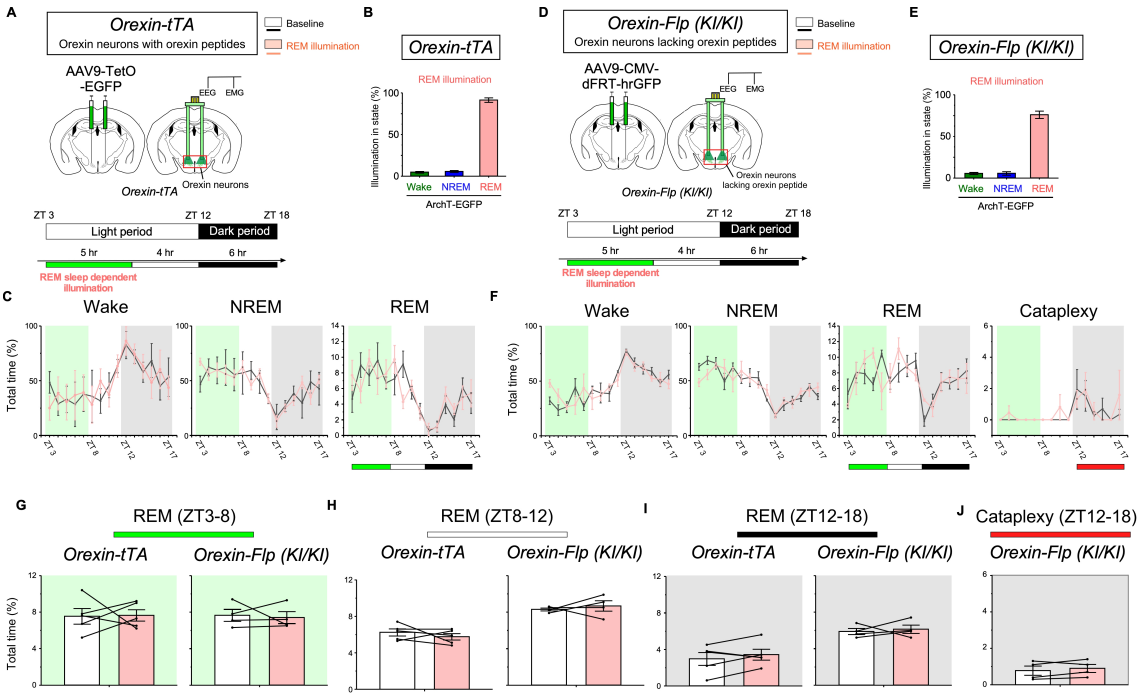

Supplementary Figure 13. REM sleep state-dependent photoillumination of orexin neurons with and without orexin peptides in EGFP and GFP control mice.

(A and D) Schematics of EGFP/hrGFP expression in orexin neurons (left) and implantation of bilateral optical fibers with EEG/EMG recordings (right) in EGFP control *orexin-tTA* mice (A) and GFP control *prepro-orexin* knockout (*orexin-Flp (KI/KI)*) mice (D). (B and E) Bar graphs indicating the illumination "cover ratio" for each vigilance state in *orexin-tTA* mice (B) and *orexin-Flp (KI/KI)* mice (E). (C and F) Line graphs showing the effects of REM sleep state-dependent illumination on the time spent in each vigilance state during REM sleep state-dependent illumination (ZT3-8), the subsequent light period (ZT8-12), and the subsequent dark period (ZT12-18) in *orexin-tTA* mice (C) and *orexin-Flp (KI/KI)* mice (F). (G-J) Bar graphs showing the effects of REM sleep state-dependent inhibition on the time spent in REM sleep and cataplexy during each time period (ZT3-8, ZT8-12, and ZT12-18) *in orexin-tTA* mice (left panels in G-I) and *prepro-orexin* knockout (*orexin-Flp (KI/KI)*) mice (right panels in G-I and J). Data are the mean ± SEM. Statistical analyses are shown in Supplementary Table 1.

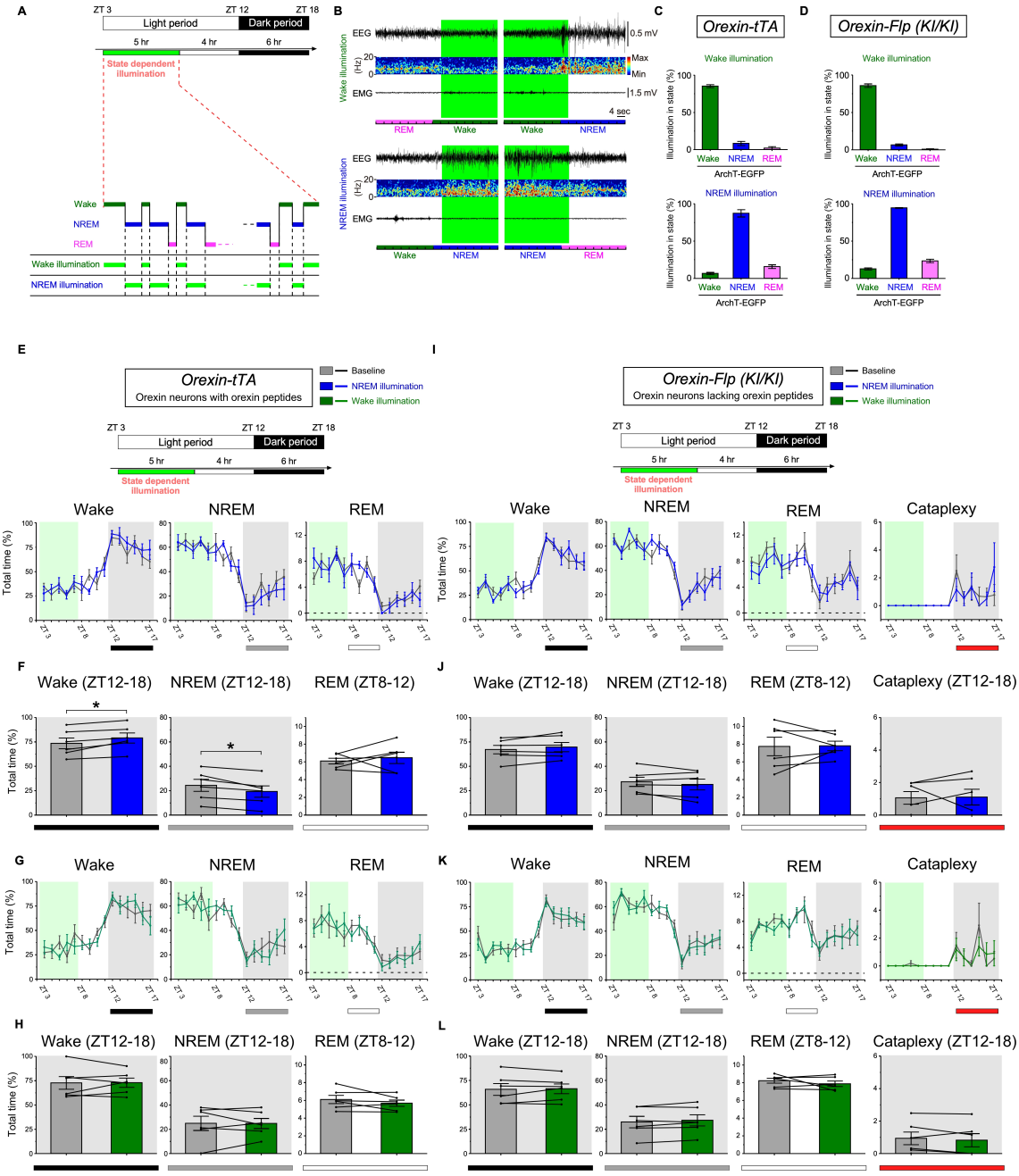

Supplementary Figure 14. State-dependent (wakefulness and NREM sleep) inhibition of orexin neurons with and without orexin peptides.

(A and B) Schematics showing an example of wakefulness or NREM sleep state-dependent illumination. (C and D) Bar graphs indicating the percentage of illumination time spent in each state in *orexin-tTA* mice (C) and orexin knockout (*orexin-Flp (KI/KI)*) mice (D). (E-L) Effects of state-dependent inhibition on the time spent in each vigilance state during state-dependent illumination (ZT3-8), the subsequent light period (ZT8-12), and the subsequent dark period (ZT12-18)

in *orexin-tTA* mice (NREM sleep state-dependent inhibition in E-F and wakefulness state-dependent inhibition in G-H) and *prepro-orexin* knockout (*orexin-Flp (KI/KI)*) mice (NREM sleep state-dependent inhibition in I-J and wakefulness state-dependent inhibition in K-L). The statistical results from other vigilance states at each time period are described in Supplementary Table 1. Data are the mean ± SEM. *P < 0.05, **P < 0.01. Statistical analyses are shown in Supplementary Table 1. FFT, fast Fourier transform; TTL, transistor-transistor logic.

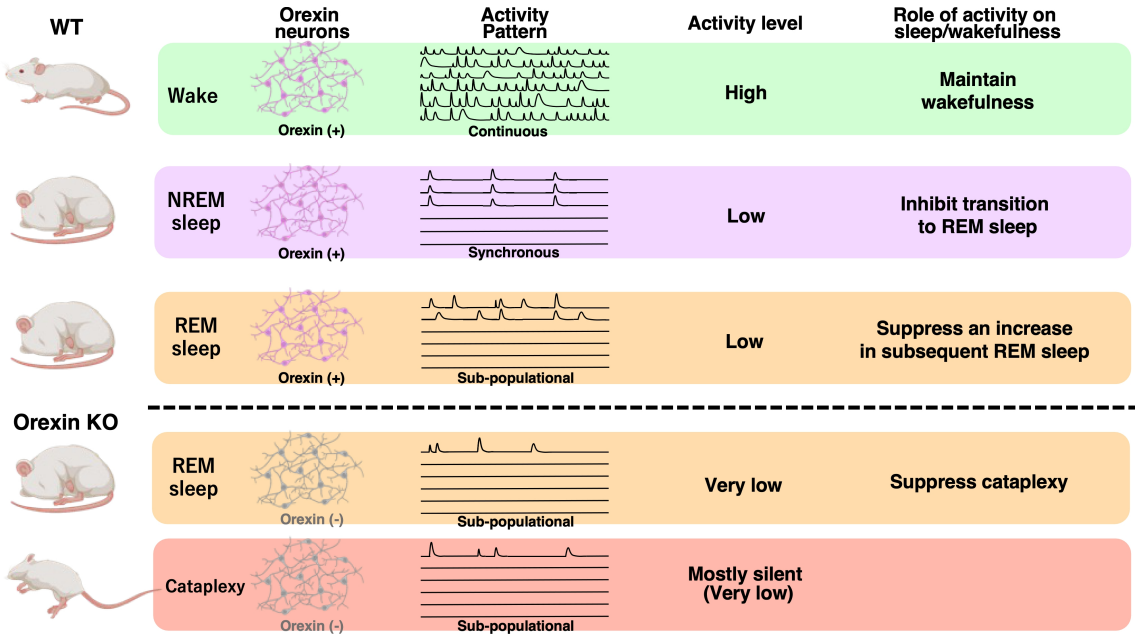

Supplementary Figure 15. Summary of results. Activity pattern of orexin neurons across sleep/wakefulness and their roles in phenotypically normal and narcolepsy model mice.

Orexin neurons were highly active during wakefulness, showed intermittent synchronous activity during NREM sleep, and a small subpopulation of these cells was active during REM sleep in phenotypically normal mice (WT). Orexin neurons that lack orexin peptides (Orexin KO mice) were less active during REM sleep compared to phenotypically normal mice (WT) and were mostly silent during cataplexy. Orexin neuron activity during NREM sleep regulates NREM-REM sleep transitions. Orexin neuron activity during REM sleep suppresses an increase in subsequent REM sleep in phenotypically normal mice (WT) but subsequent cataplexy in narcolepsy model mice (Orexin KO mice).

Movies S1. Microendoscopic Ca^{2+} imaging of orexin neurons with orexin peptides during wakefulness, NREM sleep, and REM sleep in *orexin-tTA* mice.
Representative movie shows Ca^{2+} activity from orexin neurons across vigilance states in *orexin-tTA* mice (20x speed).

Movies S2. Microendoscopic Ca^{2+} imaging of orexin neurons with orexin peptides during wakefulness, NREM sleep, and REM sleep in *orexin-Flp (KI/-)* mice.
Representative movie shows Ca^{2+} activity from orexin neurons lacking orexin peptides across vigilance states in orexin knockout (*orexin-Flp (KI/-*)) mice (20x speed).

Movies S3. Microendoscopic Ca^{2+} imaging of orexin neurons lacking orexin peptides during wakefulness, NREM sleep, and REM sleep in orexin knockout (*orexin-Flp (KI/KI)*) mice.
Representative movie shows Ca^{2+} activity from orexin neurons lacking orexin peptides across vigilance states in orexin knockout (*orexin-Flp (KI/KI*)) mice (20x speed).

Movies S4. Microendoscopic Ca^{2+} imaging of orexin neurons lacking orexin peptides during wakefulness and cataplexy in orexin knockout (*orexin-Flp (KI/KI)*) mice.
Representative movie shows Ca^{2+} activity from orexin neurons lacking orexin peptides during wakefulness and cataplexy in orexin knockout (*orexin-Flp (KI/KI*)) mice (20x speed; shown after data processing with DF/F).

Dataset S1. Dataset used in the manuscript and Figures.
The dataset which includes all data used in the manuscript and Figures is uploaded as Dataset S1.

Supplementary Table 1

Supplementary Table 1. Statistical analyses underlying Figures in the main text and supplementary information.

Figure Number	n	Normality test	Equal variance test	Statistical methods	*P* value	F/t value	Post hoc multiple comparisons test	
Figure 1D	n=6 mice	passed	failed	One-way RM ANOVA (Huynh-Feldt Epsilon) with Bonferroni post hoc comparison	P<0.001	$F_{1.9,9.6}$=428.89769	Wake vs NREM	P<0.001
							Wake vs tNR	P<0.001
							Wake vs REM	P<0.001
							NREM vs tNR	P=0.09
							tNR vs REM	P<0.015
							NREM vs REM	P=1
Figure 1F (NREM, tNR, REM)	n=6 mice	passed	passed	One-way RM ANOVA with Bonferroni post hoc comparison	P<0.001	$F_{2,10}$ = 33.01295	NREM vs tNR	P<0.001
							tNR vs REM	P<0.001
							NREM vs REM	P=0.011
Figure 2I	n=51 cells (NR-cluster cell,5 mice)	failed		Friedman's test with Bonferroni post hoc comparison	P<0.001	Chi- Square= 72.12745	NREM vs Wake	P<0.001
							Wake vs REM	P=0.038
							NREM vs REM	P<0.001
Figure 3D	n=5 mice	passed	failed	One-way RM ANOVA (Huynh-Feldt Epsilon) with Bonferroni post hoc comparison	P<0.001	$F_{1.4,5.6}$=53.50157	Wake vs NREM	P<0.001
							Wake vs tNR	P<0.001
							Wake vs REM	P<0.001
							NREM vs tNR	P=1
							tNR vs REM	P<0.16
							NREM vs REM	P=0.75
Figure 3F (NREM, tNR, REM)	n=5 mice	passed	passed	One-way RM ANOVA with Bonferroni post hoc comparison	P<0.001	$F_{2,8}$ = 27.17353	NREM vs tNR	P=0.077
							tNR vs REM	P=0.0055
							NREM vs REM	P<0.001
Figure 4I	n=34 cells (NR-cluster cell, 5 mice)	failed		Friedman's test with Bonferroni post hoc comparison	P<0.001	Chi- Square= 42.45588	NREM vs Wake	P<0.001
							Wake vs REM	P=1
							NREM vs REM	P<0.001
Figure 5C (Wake to Cataplexy)	n=5 mice	passed		Paired t test (two-tailed)	P<0.001	t_4 = 26.25629		
Figure 5C (Cataplexy to Wake)	n=5 mice	passed		Paired t test (two-tailed)	P<0.001	t_4 = -102.77863		
Figure 6E (Wake)	n=6 mice	passed		Paired t test (two-tailed)	P=0.023	t_5 = 3.24426		
Figure 6E (NREM)	n=6 mice	passed		Paired t test (two-tailed)	P=0.032	t_5 = -2.93824		
Figure 6E (REM)	n=6 mice	passed		Paired t test (two-tailed)	P=0.0084	t_5 = -4.21491		
Figure 6F	n=6 mice	passed		Paired t test (two-tailed)	P=0.023	t_5 = -3.25396		
Figure 6G (NREM to Wake)	n=6 mice	failed		Paired Wilcoxon Signed Rank test (two-tailed)	P=0.031	W= 21		
Figure 6G (Cumlative probability (NREM to Wake))	n=6 mice	failed		Gray's test	P=0.035	Chi- Square= 4.433543	Consider REM as a competing risk	
Figure 6H (NREM to REM)	n=6 mice	failed		Paired Wilcoxon Signed Rank test (two-tailed)	P=0.031	W= 0		
Figure 6H (Cumlative probability (NREM to REM))	n=6 mice	failed		Gray's test	P=0.046	Chi- Square= 3.970496	Consider Wake as a competing risk	
Figure 6M (Wake)	n=6 mice	passed		Paired t test (two-tailed)	P=0.53	t_5 = -0.68227		
Figure 6M (NREM)	n=6 mice	passed		Paired t test (two-tailed)	P=0.65	t_5 = 0.4872		
Figure 6M (REM)	n=6 mice	passed		Paired t test (two-tailed)	P=0.12	t_5 = 1.90566		
Figure 6N	n=6 mice	failed		Paired Wilcoxon Signed Rank test (two-tailed)	P=1	W=2		
Figure 6O (NREM to Wake)	n=6 mice	passed		Paired t test (two-tailed)	P=0.36	t_5 = 1.00742		
Figure 6O (Cumlative probability (NREM to Wake))	n=6 mice	failed		Gray's test	P=0.33	Chi- Square= 0.94688854	Consider REM as a competing risk	
Figure 6P (NREM to REM)	n=6 mice	passed		Paired t test (two-tailed)	P=0.36	t_5 = -1.00742		
Figure 6P (Cumlative probability (NREM to REM))	n=6 mice	failed		Gray's test	P=0.80	Chi- Square= 0.06163491	Consider Wake as a competing risk	
Figure 7B REM (ZT 3-8)	n=6 mice (Orexin-Flp(KI/KI)), n=6 mice (Orexin-tTA)	passed	passed	Unpaired t test (two-tailed)	P=0.20	t_{10} = 1.37089		
Figure 7B REM (ZT 8-12)	n=6 mice (Orexin-Flp(KI/KI)), n=6 mice (Orexin-tTA)	passed	passed	Unpaired t test (two-tailed)	P=0.013	t_{10} = -2.99627		
Figure 7B REM (ZT 12-18)	n=6 mice (Orexin-Flp(KI/KI)), n=6 mice (Orexin-tTA)	passed	passed	Unpaired t test (two-tailed)	P=0.034	t_{10} = -2.44914		
Figure 7B Wake (ZT 3-8)	n=6 mice (Orexin-Flp(KI/KI)), n=6 mice (Orexin-tTA)	failed		Mann-Whitney U test	P=1	U=18		
Figure 7B Wake (ZT 8-12)	n=6 mice (Orexin-Flp(KI/KI)), n=6 mice (Orexin-tTA)	passed	failed	Welch's t test (two-tailed)	P=0.23	$t_{6.1}$ = 1.35165		
Figure 7B Wake (ZT 12-18)	n=6 mice (Orexin-Flp(KI/KI)), n=6 mice (Orexin-tTA)	passed	passed	Unpaired t test (two-tailed)	P=0.30	t_{10} = 1.08608		
Figure 7B NREM (ZT 3-8)	n=6 mice (Orexin-Flp(KI/KI)), n=6 mice (Orexin-tTA)	passed	passed	Unpaired t test (two-tailed)	P=0.52	t_{10} = -0.66494		
Figure 7B NREM (ZT 8-12)	n=6 mice (Orexin-Flp(KI/KI)), n=6 mice (Orexin-tTA)	passed	passed	Unpaired t test (two-tailed)	P=0.53	t_{10} = -0.64404		
Figure 7B NREM (ZT 12-18)	n=6 mice (Orexin-Flp(KI/KI)), n=6 mice (Orexin-tTA)	passed	passed	Unpaired t test (two-tailed)	P=0.53	t_{10} = -0.65867		
Figure 7 REM (ZT 3-8) WT comparion in the manuscript	n=6 mice (Orexin-Flp(KI/KI)), n=7 mice (WT)	passed	passed	Unpaired t test (two-tailed)	P=0.057	t_{11} = -2.12181		
Figure 7 REM (ZT 8-12) WT comparion in the manuscript	n=6 mice (Orexin-Flp(KI/KI)), n=7 mice (WT)	passed	passed	Unpaired t test (two-tailed)	P=0.0096	t_{11} = 3.12673		
Figure 7 REM (ZT 12-18) WT comparion in the manuscript	n=6 mice (Orexin-Flp(KI/KI)), n=7 mice (WT)	passed	failed	Welch's t test (two-tailed)	P=0.0066	$t_{6.1}$ = 4.05104		
Figure 7J (left) REM illumination (Wake) ZT3-8	n=6 mice	passed		Paired t test (two-tailed)	P=0.90	t_5 = 0.12888		
Figure 7J (left) REM illumination (NREM) ZT3-8	n=6 mice	passed		Paired t test (two-tailed)	P=0.81	t_5 = -0.25302		
Figure 7J (left) REM illumination (REM) ZT3-8	n=6 mice	passed		Paired t test (two-tailed)	P=0.55	t_5 = 0.64184		
Figure 7K (left) REM illumination (Wake) ZT8-12	n=6 mice	passed		Paired t test (two-tailed)	P=0.34	t_5 = 1.06322		
Figure 7K (left) REM illumination (NREM) ZT8-12	n=6 mice	passed		Paired t test (two-tailed)	P=0.56	t_5 = -0.61715		
Figure 7K (left) REM illumination (REM) ZT8-12	n=6 mice	passed		Paired t test (two-tailed)	P=0.034	t_5 = -2.90222		
Figure 7L (left) REM illumination (Wake) ZT12-18	n=6 mice	passed		Paired t test (two-tailed)	P=0.24	t_5 = -1.33433		
Figure 7L (left) REM illumination (NREM) ZT12-18	n=6 mice	passed		Paired t test (two-tailed)	P=0.26	t_5 = 1.26266		
Figure 7L (left) REM illumination (REM) ZT12-18	n=6 mice	passed		Paired t test (two-tailed)	P=0.26	t_5 = 1.27801		
Figure 7J (right) REM illumination (Wake) ZT3-8	n=6 mice	passed		Paired t test (two-tailed)	P=0.38	t_5 = 0.96954		
Figure 7J (right) illumination (NREM) ZT3-8	n=6 mice	passed		Paired t test (two-tailed)	P=0.36	t_5 = -1.00671		
Figure 7J (right) illumination (REM) ZT3-8	n=6 mice	passed		Paired t test (two-tailed)	P=0.92	t_5 = 0.11058		
Figure 7J (right) illumination (Cataplexy) ZT3-8	n=6 mice	failed		Paired Wilcoxon Signed Rank test (two-tailed)	P=1	W= 0		
Figure 7K (right) REM illumination (Wake) ZT8-12	n=6 mice	passed		Paired t test (two-tailed)	P=0.32	t_5 = 1.10092		
Figure 7K (right) REM illumination (NREM) ZT8-12	n=6 mice	passed		Paired t test (two-tailed)	P=0.20	t_5 = -1.48656		
Figure 7K (right) REM illumination (REM) ZT8-12	n=6 mice	passed		Paired t test (two-tailed)	P=0.91	t_5 = 0.11576		
Figure 7K (right) REM illumination (Cataplexy) ZT8-12	n=6 mice	failed		Paired Wilcoxon Signed Rank test (two-tailed)	P=1	W= 0		
Figure 7L (right) REM illumination (Wake) ZT12-18	n=6 mice	passed		Paired t test (two-tailed)	P=0.22	t_5 = -1.40612		
Figure 7L (right) REM illumination (NREM) ZT12-18	n=6 mice	passed		Paired t test (two-tailed)	P=0.088	t_5 = 2.11401		
Figure 7L (right) REM illumination (REM) ZT12-18	n=6 mice	passed		Paired t test (two-tailed)	P=0.58	t_5 = 0.5928		
Figure 7M REM illumination (Cataplexy) ZT12-18	n=6 mice	passed		Paired t test (two-tailed)	P=0.0069	t_5 = -4.4249		

S. Figure 1D (delta)	n=6 mice	passed	failed	One-way RM ANOVA (Huynh-Feldt Epsilon) with Bonferroni post hoc comparison	P=0.10	$F_{1.2,6.1}$ = 3.64513	High vs Low	P=0.10
							Middle vs Low	P=1
							High vs Middle	P=0.15
S. Figure 1D (theta)	n=6 mice	passed	passed	One-way RM ANOVA with Bonferroni post hoc comparison	P<0.001	$F_{2,10}$ =73.11996	High vs Low	P<0.001
							Middle vs Low	P=0.0044
							High vs Middle	P<0.001
S. Figure 1D (alpha)	n=6 mice	passed	failed	One-way RM ANOVA (Huynh-Feldt Epsilon) with Bonferroni post hoc comparison	P<0.001	$F_{1.2,6.0}$ = 110.69742	High vs Low	P<0.001
							Middle vs Low	P<0.001
							High vs Middle	P<0.001
S. Figure 1F (Wake to NREM)	n=6 mice	passed		Paired t test (two-tailed)	P<0.001	t_5 = 31.25004		
S. Figure 1F (NREM to Wake)	n=6 mice	passed		Paired t test (two-tailed)	P<0.001	t_5 = -34.72768		
S. Figure 1F (REM to Wake)	n=6 mice	passed		Paired t test (two-tailed)	P<0.001	t_5 = -20.4024		
S. Figure 1H	n=6 mice	passed	passed	One-way RM ANOVA with Bonferroni post hoc comparison	P<0.001	$F_{2,10}$ = 441.39007	Wake (pre) vs MA	P<0.001
							MA vs Wake (Post)	P<0.001
							Wake (pre) vs Wake (post)	P=1
S. Figure 3I	n=39 cells (NR-cluster cell, 3 mice)	failed		Friedman's test with Bonferroni post hoc comparison	P<0.001	Chi- Square= 64.97436	NREM vs Wake	P<0.001
							Wake vs REM	P=0.041
							NREM vs REM	P<0.001
S. Figure 4B	KI/KI, n=6 cells KI/-, n=8 cells	passed	failed	one-way RM ANOVA (Huynh-Feldt Epsilon) with Bonferroni's multiple comparison test	p<0.001	KI/KI,$F_{1.1,5.3}$=6.05111 KI/-,$F_{1.1,7.5}$=18.566	5 Hz vs 10 Hz : KI/KI(P=1); KI/-(P=1) 5 Hz vs 20 Hz :KI/KI(P=1);KI/-(P=0.05459) 5 Hz vs 50 Hz :KI/KI(P<0.001);KI/-(P<0.001) 10 Hz vs 20 Hz : KI/KI(P=1);KI/-(P=0.49599) 10 Hz vs 50 Hz : KI/KI(P<0.001);KI/-(P<0.001) 20 Hz vs 50 Hz : KI/KI(P=0.10683);KI/-(P<0.001)	
S. Figure 4E	KI/KI, n=11 cells KI/-, n=9 cells	failed		Friedman's test with Bonferroni's multiple comparison test	p<0.001	KI/KI,Chi-Square=22.13318 KI/-, Chi-Squre=9.20312	10 uM vs 50 uM : KI/KI(P=0.06752); KI/-(P=0.20917 10 uM vs 100 uM :KI/KI(P<0.001); KI/-(P<0.001) 10 uM vs 1000 uM : KI/KI(P<0.001); KI/-(P<0.001) 50 uM vs 100 uM : KI/KI(P=0.05224); KI/-(P=0.02424) 50 uM vs 1000 uM : KI/KI(P<0.001); KI/-(P<0.001) 100 uM vs 1000 uM : KI/KI(P<0.001); KI/-(P<0.001)	
S. Figure 5D (delta)	n=5 mice	passed	failed	One-way RM ANOVA (Huynh-Feldt Epsilon) with Bonferroni post hoc comparison	P=0.30	$F_{1.1,4.6}$ = 1.40158	High vs Low	P=0.43
							Middle vs Low	P=0.83
							High vs Middle	P=1
S. Figure 5D (theta)	n=5 mice	passed	failed	One-way RM ANOVA (Huynh-Feldt Epsilon) with Bonferroni post hoc comparison	P=0.012	$F_{1.0,4.1}$ = 17.98205	High vs Low	P=0.0010
							Middle vs Low	P=0.15
							High vs Middle	P=0.019
S. Figure 5D (alpha)	n=5 mice	passed	passed	One-way RM ANOVA with Bonferroni post hoc comparison	P<0.001	$F_{2,8}$ = 40.5141	High vs Low	P<0.001
							Middle vs Low	P=0.027
							High vs Middle	P=0.0017
S. Figure 5F (Wake to NREM)	n=5 mice	passed		Paired t test (two-tailed)	P<0.001	t_4 = 25.53353		
S. Figure 5F (NREM to Wake)	n=5 mice	passed		Paired t test (two-tailed)	P<0.001	t_4 = -75.23121		
S. Figure 5F (REM to Wake)	n=5 mice	passed		Paired t test (two-tailed)	P<0.001	t_4 = -26.74194		
S. Figure 5H	n=5 mice	passed	failed	One-way RM ANOVA (Huynh-Feldt Epsilon) with Bonferroni post hoc comparison	P=0.0019	$F_{1.0,4.2}$ = 48.49734	Wake (pre) vs MA	P<0.001
							MA vs Wake (Post)	P<0.001
							Wake (pre) vs Wake (post)	P=1
S. Figure 6D	n=43 cells (3 mice)	failed		Paired Wilcoxon Signed Rank test (two-tailed)	P=0.80	W=410		
S. Figure 7E	n=12 cells	passed	passed	one-way RM ANOVA with Bonferroni's multiple comparison test	p<0.001	$F_{2,22}$ = 71.75018	Pre vs sti : p<0.001 Pre vs post : p=0.0531 Sti vs post : p<0.001	
S. Figure 7F	n=12 cells	passed	passed	one-way RM ANOVA with Bonferroni's multiple comparison test	p=0.0041	$F_{2,22}$ = 7.14518	Pre vs sti : p<0.001 Pre vs post : p=0.22439 Sti vs post : p=0.20784	
S. Figure 8C (Wake)	n=5 mice	passed		Paired t test (two-tailed)	P=0.89	t_4 = -0.14655		
S. Figure 8C (NREM)	n=5 mice	passed		Paired t test (two-tailed)	P=0.80	t_4 = 0.27149		
S. Figure 8C (REM)	n=5 mice	passed		Paired t test (two-tailed)	P=0.72	t_4 = -0.39119		
S. Figure 8D	n=5 mice	failed		Paired Wilcoxon Signed Rank test (two-tailed)	P=0.37	W=0		
S. Figure 8E	n=5 mice	passed		Paired t test (two-tailed)	P=0.79	t_4 = 0.28769		
S. Figure 8E (NREM to Wake)	n=5 mice	passed		Paired t test (two-tailed)	P=0.79	t_4 = -0.28769		
S. Figure 8H (Wake)	n=4 mice	passed		Paired t test (two-tailed)	P=0.76	t_3 =-0.34068		
S. Figure 8H (NREM)	n=4 mice	passed		Paired t test (two-tailed)	P=0.75	t_3 = 0.3551		
S. Figure 8H (REM)	n=4 mice	passed		Paired t test (two-tailed)	P=0.88	t_3 = 0.15207		
S. Figure 8I	n=4 mice	failed		Paired Wilcoxon Signed Rank test (two-tailed)	P=0.35	W=3		
S. Figure 8J (NREM to REM)	n=4 mice	passed		Paired t test (two-tailed)	P=0.74	t_3 = -0.3694		
S. Figure 8J (NREM to Wake)	n=4 mice	passed		Paired t test (two-tailed)	P=0.74	t_3 = 0.3694		
S. Figure 9A Wake (delta)	n=6 mice	passed		Paired t test (two-tailed)	P=0.14	t_5 = 1.75978		
S. Figure 9A Wake (theta)	n=6 mice	passed		Paired t test (two-tailed)	P=0.41	t_5 = 0.19627		
S. Figure 9A Wake (alpha)	n=6 mice	passed		Paired t test (two-tailed)	P=0.31	t_5 = 1.13324		
S. Figure 9A NREM (delta)	n=6 mice	passed		Paired t test (two-tailed)	P=0.13	t_5 = -1.79484		
S. Figure 9A NREM (theta)	n=6 mice	passed		Paired t test (two-tailed)	P=0.12	t_5 = -1.88614		
S. Figure 9A NREM (alpha)	n=6 mice	passed		Paired t test (two-tailed)	P=0.066	t_5 = -2.35082		
S. Figure 9A REM (delta)	n=6 mice	passed		Paired t test (two-tailed)	P=0.10	t_4 = -2.11149		
S. Figure 9A REM (theta)	n=6 mice	passed		Paired t test (two-tailed)	P=0.15	t_4 = -1.76677		
S. Figure 9A REM (alpha)	n=6 mice	passed		Paired t test (two-tailed)	P=0.14	t_4 = -1.84968		
S. Figure 9B Wake (delta)	n=6 mice	passed		Paired t test (two-tailed)	P=0.32	t_5 = -1.10057		
S. Figure 9B Wake (theta)	n=6 mice	passed		Paired t test (two-tailed)	P=0.20	t_5 = -1.48269		
S. Figure 9B Wake (alpha)	n=6 mice	passed		Paired t test (two-tailed)	P=0.74	t_5 = -0.34661		
S. Figure 9B NREM (delta)	n=6 mice	passed		Paired t test (two-tailed)	P=0.42	$t_{5.}$ -0.87045		
S. Figure 9B NREM (theta)	n=6 mice	passed		Paired t test (two-tailed)	P=0.23	t_5 =1.35169		
S. Figure 9B NREM (alpha)	n=6 mice	passed		Paired Wilcoxon Signed Rank test (two-tailed)	P=0.06	W= 20		
S. Figure 9B REM (delta)	n=6 mice	passed		Paired t test (two-tailed)	P=0.055	t_5 = 2.68971		
S. Figure 9B REM (theta)	n=6 mice	passed		Paired t test (two-tailed)	P=0.79	t_5 = -0.29231		
S. Figure 9B REM (alpha)	n=6 mice	passed		Paired t test (two-tailed)	P=0.25	t_5 = -1.339		
S. Figure 10D	n=12 cells	passed	passed	one-way RM ANOVA with Bonferroni's multiple comparison test	p<0.001	$F_{2,22}$ = 127.750	Pre vs sti : p<0.001 Pre vs post : p=0.33683 Sti vs post : p<0.001	
S. Figure 10F (Wake)	n=4 mice	passed		Paired t test (two-tailed)	P=0.056	t_3 =-3.04193		
S. Figure 10F (NREM)	n=4 mice	passed		Paired t test (two-tailed)	P=0.15	t_3 = 1.93826		
S. Figure 10F (REM)	n=4 mice	passed		Paired t test (two-tailed)	P=0.022	t_3 = 4.38342		
S. Figure 10G (Wake, duration)	n=4 mice	passed		Paired t test (two-tailed)	P=0.12	t_3 = -2.16589		
S. Figure 10G (NREM, duration)	n=4 mice	passed		Paired t test (two-tailed)	P=0.24	t_3 = 1.45244		
S. Figure 10G (REM, duration)	n=4 mice	passed		Paired t test (two-tailed)	P=0.60	t_3 = 0.57792		
S. Figure 10H (NREM to REM)	n=4 mice	passed		Paired t test (two-tailed)	P=0.023	t_3 = 4.30734		
S. Figure 10H (NREM to Wake)	n=4 mice	passed		Paired t test (two-tailed)	P=0.023	t_3 = -4.30734		
S. Figure 10H (Cumlative probability (NREM to REM))	n=4 mice	failed		Gray's test	P=0.0095	Chi- Square= 6.737333	Consider Wake as a competing risk	
S. Figure 10H (Cumlative probability (NREM to Wake))	n=4 mice	failed		Gray's test	P=0.015	Chi- Square= 5.969562	Consider REM as a competing risk	

S. Figure 11F	n=11 cells (n=3 mice)	passed	passed	One-way RM ANOVA with Tukey's multiple comparison test	p<0.001	$F_{2,20}$ = 31.22186	Pre vs sti : p<0.001 Pre vs post : p=0.26373 Sti vs post : p<0.001	
S. Figure 11G	n=11 cells (n=3 mice)	passed	passed	One-way RM ANOVA with Tukey's multiple comparison test	p<0.001	$F_{2,20}$ = 10.0895	Pre vs sti : p<0.001 Pre vs post : p=0.63817 Sti vs post : p<0.001	
S. Figure 12G (left) REM illumination (Wake) vs. Yoked control ZT3-8	n=6 mice	passed		Paired t test (two-tailed)	P=0.41	t_5 = -0.89624		
S. Figure 12G (left) REM illumination (NREM) vs. Yoked control ZT3-8	n=6 mice	passed		Paired t test (two-tailed)	P=0.35	t_5 = 1.03034		
S. Figure 12G (left) REM illumination (REM) vs. Yoked control ZT3-8	n=6 mice	passed		Paired t test (two-tailed)	P=0.79	t_5 = 0.28507		
S. Figure 12H (left) REM illumination (Wake) vs. Yoked control ZT8-12	n=6 mice	passed		Paired t test (two-tailed)	P=0.013	t_5 = 3.71513		
S. Figure 12H (left) REM illumination (NREM) vs. Yoked control ZT8-12	n=6 mice	passed		Paired t test (two-tailed)	P=0.019	t_5 = -3.42581		
S. Figure 12H (left) REM illumination (REM) vs. Yoked control ZT8-12	n=6 mice	passed		Paired t test (two-tailed)	P=0.027	t_5 = -3.10551		
S. Figure 12I (left) REM illumination (Wake) vs. Yoked control ZT12-18	n=6 mice	passed		Paired t test (two-tailed)	P=0.48	t_5 = -0.75922		
S. Figure 12I (left) REM illumination (NREM) vs. Yoked control ZT12-18	n=6 mice	passed		Paired t test (two-tailed)	P=0.58	t_5 = 0.59728		
S. Figure 12I (left) REM illumination (REM) vs. Yoked control ZT12-18	n=6 mice	passed		Paired t test (two-tailed)	P=0.55	t_5 = 0.6401		
S. Figure 12G (right) REM illumination (Wake) vs. Yoked control ZT3-8	n=6 mice	passed		Paired t test (two-tailed)	P=0.67	t_5 = 0.45124		
S. Figure 12G (right) REM illumination (NREM) vs. Yoked control ZT3-8	n=6 mice	passed		Paired t test (two-tailed)	P=0.41	t_5 = -0.8916		
S. Figure 12G (right) illumination (REM) vs. Yoked control ZT3-8	n=6 mice	passed		Paired t test (two-tailed)	P=0.12	t_5 = 1.84677		
S. Figure 12G (right) illumination (Cataplexy) vs. Yoked control ZT3-8	n=6 mice	failed		Paired Wilcoxon Signed Rank test (two-tailed)	P=1	W= 0		
S. Figure 12H (right) illumination (Wake) vs. Yoked control ZT8-12	n=6 mice	passed		Paired t test (two-tailed)	P=0.90	t_5 = 0.12842		
S. Figure 12H (right) REM illumination (NREM) vs. Yoked control ZT8-12	n=6 mice	passed		Paired t test (two-tailed)	P=0.48	t_5 = -0.77136		
S. Figure 12H (right) REM illumination (REM) vs. Yoked control ZT8-12	n=6 mice	passed		Paired t test (two-tailed)	P=0.52	t_5 = -0.70066		
S. Figure 12H (right) REM illumination (Cataplexy) vs. Yoked control ZT8-12	n=6 mice	failed		Paired Wilcoxon Signed Rank test (two-tailed)	P=1	W=0		
S. Figure 12I (right) REM illumination (Wake) vs. Yoked control ZT12-18	n=5 mice	passed		Paired t test (two-tailed)	P=0.16	t_4 = 1.67014		
S. Figure 12I (right) REM illumination (NREM) vs. Yoked control ZT12-18	n=5 mice	passed		Paired t test (two-tailed)	P=0.48	t_4 = -0.76817		
S. Figure 12I (right) REM illumination (REM) vs. Yoked control ZT12-18	n=5 mice	passed		Paired t test (two-tailed)	P=0.85	t_4 = -0.19835		
S. Figure 12J (right) REM illumination (Cataplexy) vs. Yoked control ZT12-18	n=5 mice	passed		Paired t test (two-tailed)	P=0.0084	t_4 = -4.20758		
S. Figure 13G (left) REM illumination (REM) ZT3-8	n=5 mice	passed		Paired t test (two-tailed)	P=0.77	t_4 = -0.31954		
S. Figure 13H (left) REM illumination (REM) ZT8-12	n=5 mice	passed		Paired t test (two-tailed)	P=0.94	t_4 = -0.08103		
S. Figure 13I (left) REM illumination (REM) ZT12-18	n=5 mice	failed		Paired Wilcoxon Signed Rank test (two-tailed)	P=0.31	W=12		
S. Figure 13G (right) illumination (REM) ZT3-8	n=4 mice	passed		Paired t test (two-tailed)	P=0.80	t_3 = 0.27538		
S. Figure 13H (right) REM illumination (REM) ZT8-12	n=4 mice	passed		Paired t test (two-tailed)	P=0.63	t_3 = 0.5428		
S. Figure 13I (right) REM illumination (REM) ZT12-18	n=4 mice	passed		Paired t test (two-tailed)	P=0.73	t_3 = -0.37941		
S. Figure 13J (right) REM illumination (Cataplexy) ZT12-18	n=4 mice	passed		Paired t test (two-tailed)	P=0.37	t_3 = -1.05802		
S. Figure 14F NREM illumination (Wake) ZT3-8	n=6 mice	passed		Paired t test (two-tailed)	P=0.77	t_5 = -0.30573		
S. Figure 14F NREM illumination (NREM) ZT3-8	n=6 mice	passed		Paired t test (two-tailed)	P=0.71	t_5 = 0.39201		
S. Figure 14F NREM illumination (REM) ZT3-8	n=6 mice	passed		Paired t test (two-tailed)	P=0.86	t_5 = -0.19137		
S. Figure 14F NREM illumination (Wake) ZT8-12	n=6 mice	passed		Paired t test (two-tailed)	P=0.64	t_5 = 0.49733		
S. Figure 14F NREM illumination (NREM) ZT8-12	n=6 mice	passed		Paired t test (two-tailed)	P=0.69	t_5 = -0.42519		
S. Figure 14F NREM illumination (REM) ZT8-12	n=6 mice	passed		Paired t test (two-tailed)	P=0.59	t_5 = -0.57698		
S. Figure 14F NREM illumination (Wake) ZT12-18	n=6 mice	passed		Paired t test (two-tailed)	P=0.012	t_5 = -3.88207		
S. Figure 14F NREM illumination (NREM) ZT12-18	n=6 mice	failed		Paired Wilcoxon Signed Rank test (two-tailed)	P=0.031	W= 21		
S. Figure 14F NREM illumination (REM) ZT12-18	n=6 mice	passed		Paired t test (two-tailed)	P=0.21	t_5 =1.43362		
S. Figure 14H Wake illumination (Wake) ZT3-8	n=6 mice	passed		Paired t test (two-tailed)	P=0.36	t_5 = 1.00619		
S. Figure 14H Wake illumination (NREM) ZT3-8	n=6 mice	passed		Paired t test (two-tailed)	P=0.66	t_5 = -0.46567		
S. Figure 14H Wake illumination (REM) ZT3-8	n=6 mice	passed		Paired t test (two-tailed)	P=0.30	t_5 = -1.16854		
S. Figure 14H Wake illumination (Wake) ZT8-12	n=6 mice	passed		Paired t test (two-tailed)	P=0.63	t_5 = 0.51532		
S. Figure 14H Wake illumination (NREM) ZT8-12	n=6 mice	passed		Paired t test (two-tailed)	P=0.55	t_5 = -0.6418		
S. Figure 14H Wake illumination (REM) ZT8-12	n=6 mice	passed		Paired t test (two-tailed)	P=0.24	t_5 = 1.31863		
S. Figure 14H Wake illumination (Wake) ZT12-18	n=6 mice	passed		Paired t test (two-tailed)	P=0.95	t_5 = -0.06596		
S. Figure 14H Wake illumination (NREM) ZT12-18	n=6 mice	passed		Paired t test (two-tailed)	P=0.98	t_5 = 0.03043		
S. Figure 14H Wake illumination (REM) ZT12-18	n=6 mice	passed		Paired t test (two-tailed)	P=0.75	t_5 = 0.3325		
S. Figure 14J NREM illumination (Wake) ZT3-8	n=6 mice	passed		Paired t test (two-tailed)	P=0.56	t_5 = -0.62283		
S. Figure 14J NREM illumination (NREM) ZT3-8	n=6 mice	passed		Paired t test (two-tailed)	P=0.51	t_5 = -0.70781		
S. Figure 14J NREM illumination (REM) ZT3-8	n=6 mice	passed		Paired t test (two-tailed)	P=0.23	t_5 = 1.35264		
S. Figure 14J NREM illumination (Cataplexy) ZT3-8	n=6 mice	failed		Paired Wilcoxon Signed Rank test (two-tailed)	P=1	W= 0		
S. Figure 14J NREM illumination (Wake) ZT8-12	n=6 mice	passed		Paired t test (two-tailed)	P=0.25	t_5 = 1.30115		
S. Figure 14J NREM illumination (NREM) ZT8-12	n=6 mice	passed		Paired t test (two-tailed)	P=0.21	t_5 = -1.43629		
S. Figure 14J NREM illumination (REM) ZT8-12	n=6 mice	passed		Paired t test (two-tailed)	P=0.93	t_5 = -0.09922		
S. Figure 14J NREM illumination (Cataplexy) ZT8-12	n=6 mice	failed		Paired Wilcoxon Signed Rank test (two-tailed)	P=1	W= 0		
S. Figure 14J NREM illumination (Wake) ZT12-18	n=6 mice	passed		Paired t test (two-tailed)	P=0.18	t_5 = -1.54439		
S. Figure 14J NREM illumination (NREM) ZT12-18	n=6 mice	passed		Paired t test (two-tailed)	P=0.28	t_5 = 1.22371		
S. Figure 14J NREM illumination (REM) ZT12-18	n=6 mice	passed		Paired t test (two-tailed)	P=0.26	t_5 = 1.25876		
S. Figure 14J NREM illumination (Cataplexy) ZT12-18	n=6 mice	passed		Paired t test (two-tailed)	P=0.89	t_5 = -0.14704		
S. Figure 14L Wake illumination (Wake) ZT3-8	n=6 mice	passed		Paired t test (two-tailed)	P=0.31	t_5 = 1.14208		
S. Figure 14L Wake illumination (NREM) ZT3-8	n=6 mice	passed		Paired t test (two-tailed)	P=0.23	t_5 = -1.38049		
S. Figure 14L Wake illumination (REM) ZT3-8	n=6 mice	passed		Paired t test (two-tailed)	P=0.34	t_5 = 1.05593		
S. Figure 14L Wake illumination (Cataplexy) ZT3-8	n=6 mice	failed		Paired Wilcoxon Signed Rank test (two-tailed)	P=1	W=0		
S. Figure 14L Wake illumination (Wake) ZT8-12	n=6 mice	passed		Paired t test (two-tailed)	P=0.41	t_5 = -0.89658		
S. Figure 14L Wake illumination (NREM) ZT8-12	n=6 mice	passed		Paired t test (two-tailed)	P=0.55	t_5 = 0.64692		
S. Figure 14L Wake illumination (REM) ZT8-12	n=6 mice	passed		Paired t test (two-tailed)	P=0.39	t_5 = 0.9484		
S. Figure 14L Wake illumination (Cataplexy) ZT8-12	n=6 mice	failed		Paired Wilcoxon Signed Rank test (two-tailed)	P=1	W= 0		
S. Figure 14L Wake illumination (Wake) ZT12-18	n=6 mice	passed		Paired t test (two-tailed)	P=0.76	t_5 = -0.32215		
S. Figure 14L Wake illumination (NREM) ZT12-18	n=6 mice	passed		Paired t test (two-tailed)	P=0.18	t_5 = -1.55271		
S. Figure 14L Wake illumination (REM) ZT12-18	n=6 mice	passed		Paired t test (two-tailed)	P=0.79	t_5 = -0.28025		
S. Figure 14L Wake illumination (Cataplexy) ZT12-18	n=6 mice	passed		Paired t test (two-tailed)	P=0.39	t_5 = 0.93675		

Supplementary Table 2

Supplementary Table 2. Vigilance state of phenotypically normal *orexin-tTA* mice and narcoleptic *orexin-Flp (KI/KI)* mice used in the fiberphotometry experiments.

	REM sleep			NREM sleep			Wake			Cataplexy
	Orexin-tTA	Orexin-Flp(KI/KI)	P	Orexin-tTA	Orexin-Flp(KI/KI)	P	Orexin-tTA	Orexin-Flp(KI/KI)	P	Orexin-Flp(KI/KI)
24 hour										
Total time (%,±SEM)	5.5 ± 0.3	5.9 ± 0.5	n.s.	42.3 ± 1.3	41.4 ± 2.4	n.s.	52.3 ± 1.3	51.8 ± 2.5	n.s.	0.8 ± 0.2
Duration (sec,±SEM)	78.3 ± 4.0	62.5 ± 3.8	0.019	78.4 ± 5.7	70.4 ± 1.4	n.s.	97.8 ± 9.4	88.4 ± 8.5	n.s.	92.7 ± 12.0
Bout (number,±SEM)	61.3 ± 5.0	82.8 ± 8.3	0.046	480.7 ± 42.8	509.2 ± 29.8	n.s.	481.3 ± 42.8	517.4 ± 28.5	n.s.	7.8 ± 2.2
REM latency (sec, ±SEM)	29.9 ± 2.9	23.9 ± 0.9	0.11							

Vigilance state parameters of phenotypically normal *orexin-tTA* mice (n=6) and narcoleptic orexin-Flp (KI/KI) mice (n=5) in the fiberphotometry experiments. To evaluate NREM sleep without microarousal in the fiber photometry experiments, we classified brief episodes of wakefulness (~4 sec) flanked by NREM sleep as wakefulness with epochs located on both sides. Chocolate was provided for at least 3 days during habituation and before recording in *orexin-Flp (KI/KI)* mice to induce cataplexy, but not in *orexin-tTA* mice. Wake, Wakefulness.

Supplementary Table 3

Supplementary Table 3. Vigilance state in the 10 min episodes for Z-score (all stages) in *orexin-tTA* mice and *orexin-Flp (KI/KI)* mice

	Orexin-tTA	Orexin-Flp(KI/KI)	p
Total time (sec ,±SEM)			
Wake	164.1 ± 13.3	192.9 ± 13.7	n.s.
NREM sleep	115.4 ± 9.1	99.2 ± 3.4	n.s.
REM sleep	99.6 ± 2.8	96.0 ± 3.9	n.s.

Vigilance state parameters in the 10 mins' episodes for Z-score (all stages) in *orexin-tTA* mice (n=6) and *orexin-Flp (KI/KI*) mice (n=5) . To evaluate NREM sleep without microarousal in the fiber photometry experiments, we classified brief episodes of wakefulness (~4 sec) flanked by NREM sleep as wakefulness with epochs located on both sides. Chocolate was provided for at least 3 days during habituation and before recording in *orexin-Flp (KI/KI)* mice to induce cataplexy, but not in *orexin-tTA* mice. Wake, Wakefulness.

Reference

1. S. Tabuchi *et al.*, Conditional ablation of orexin/hypocretin neurons: a new mouse model for the study of narcolepsy and orexin system function. *J Neurosci* **34**, 6495-6509 (2014).
2. S. Chowdhury *et al.*, Dissociating orexin-dependent and -independent functions of orexin neurons using novel Orexin-Flp knock-in mice. *Elife* **8** (2019).
3. K. F. Tanaka *et al.*, Expanding the repertoire of optogenetically targeted cells with an enhanced gene expression system. *Cell Rep* **2**, 397-406 (2012).
4. S. Izawa *et al.*, REM sleep-active MCH neurons are involved in forgetting hippocampus-dependent memories. *Science* **365**, 1308-1313 (2019).
5. A. Inutsuka *et al.*, The integrative role of orexin/hypocretin neurons in nociceptive perception and analgesic regulation. *Sci Rep* **6**, 29480 (2016).
6. I. Tobler, T. Deboer, M. Fischer, Sleep and sleep regulation in normal and prion protein-deficient mice. *J Neurosci* **17**, 1869-1879 (1997).
7. A. Vassalli *et al.*, Electroencephalogram paroxysmal theta characterizes cataplexy in mice and children. *Brain* **136**, 1592-1608 (2013).
8. E. A. Mukamel, A. Nimmerjahn, M. J. Schnitzer, Automated analysis of cellular signals from large-scale calcium imaging data. *Neuron* **63**, 747-760 (2009).
9. K. Ghandour *et al.*, Orchestrated ensemble activities constitute a hippocampal memory engram. *Nat Commun* **10**, 2637 (2019).